Diplomarbeit

Master's Thesis

Identification of plastic material parameters from spherical penetration tests

Ermittlung plastischer Materialparameter auf Basis kugelförmiger Penetrationsversuche

Ausgeführt zum Zwecke der Erlangung des akademischen Grades eines Diplom-Ingenieurs

am

Institut für Mechanik der Werkstoffe und Strukturen

der

Technischen Universität Wien
Fakultät für Bauingenieurwesen

unter Anleitung von

Dipl.-Ing. Dr.techn. Andreas Jäger
Univ.Prof. Dipl.-Ing. Dr.techn. Roman Lackner

durch

Thomas Niederkofler
Matr.Nr.:9626102
Hernstorferstr. 3/8
1140 Wien

Wien, im Oktober 2008 .....

Danksagung

Bedanken möchte ich mich bei Univ.Prof. Dipl.-Ing. Dr.techn. Roman Lackner sowie bei meinen Diplomarbeitsbetreuer Dipl.-Ing. Dr.techn Andreas Jäger für die Ausdauer und Unterstützung.

Weiters möchte ich mich bei meinen Eltern Marianne und Richard Niederkofler - ohne Ihren Beistand wäre mein Studium nicht möglich gewesen - sowie meiner Schwester Dr. Vera Niederkofler bedanken.

Nicht zu vergessen sind Alex Oismüller, Jan Höbart, Michael Fister, Peter Haas, Bernhard Höfer, Mikko Anttila, Jusso Rautkylä, die mir eine schöne aber auch dementsprechend lange Studienzeit ermöglichten.

In besonderem Maße möchte ich mich bei meiner Freundin Rosemarie Wiesinger für Ihre Leidensfähigkeit und Unterstützung bedanken.

Kurzfassung

Mit Hilfe der Methode der finiten Elemente Methoden wurden kugelförmige Penetrationsversuche unter Berücksichtigung elastischer und elasto-plastischer Materialeigenschaften sowie verschiedener Kugelradien simuliert. Sowohl die erhaltenen Ergebnisse als auch die analytischen Lösungen nach Hertz und Sneddon wurden in dimensionsloser Form dargestellt (Π_P und Π_h).

Bei der numerischen Simulation für elastisches Materialverhalten lag der dimensionslose Parameter Π_P immer über dem entsprechenden Wert der analytischen Lösung, was auf die Vernachlässigung von radialen Deformationen der Punkte entlang der Kontaktfläche in der analytischen Lösung zurückzuführen war. Die gewonnen numerischen Ergebnisse erlaubten die anschließende Korrektur der analytischen Lösungen.

Bei der Simulation des elasto-plastischen Materialverhaltens wurden neben unterschiedlicher Kugelradien und Querdehnzahlen auch die Auswirkung der Fließgrenze untersucht. Die Ergebnisse zeigten, dass für ein konstantes Fließgrenze/Elastizitätsmodul-Verhältnis der dimensionslose Parameter Π_P aufgrund der gewählten dimensionslosen Darstellung mit einer Funktion, die unabhängig vom Kugelradius ist, beschrieben werden kann.

Auf Basis der gewonnenen funktionellen Zusammenhänge kann an Hand experimenteller Ergebnisse von Penetrationsversuchen auf die Fliesgrenze bzw. den Elastizitätsmodul des untersuchten Materials geschlossen werden.

Abstract

The finite element method was employed for the simulation of spherical penetration experiments considering elastic and elasto-plastic material behavior as well as different sphere radii. The obtained results and the analytical solutions according to Hertz and Sneddon were represented in a dimensionless form (Π_P und Π_h).

The results of the numerical simulation considering elastic material response showed that the dimensionless parameter Π_P exceeds the value of Π_P given by the analytical solution. This effect is explained by neglecting radial displacement of points along the surface of contact in the analytical solution. The obtained numerical results were used to correct the analytical solution.

In the simulations considering elasto-plastic material behavior, the influence of different intender radii, Poisson's ratios, and yield strengths was investigated. The results showed that – due to the chosen dimensionless representation - Π_P can be described as a function of the yield-strength/Young's-modulus ratio, being independent of the selected sphere radius.

Based on the obtained correlations, experimental data from penetration tests may be used for determining yield strength and Young's modulus of the investigated material sample.

Contents

1 Motivation

Instrumented indentation is a well known tool for the finer-scale characterization of materials at various length scales, from the nanometer to the millimeter range. During indentation tests, a tip with defined shape penetrates the specimen surface with the indentation load *P* [N] and the penetration *h* [m] recorded as a function of time. Commonly, each indent consists of a loading, holding, and unloading phase (see Figure 1-1). In the most general case, the material response is characterized by elastic, plastic, and viscous behavior. Elastic parameters are determined from the unloading branch of the load-penetration history under the assumption of purely elastic unloading [Oliver and Pharr 1992]. Parameter identification of materials exhibiting time-dependent behavior (e.g., polymers, bitumen, etc.) requires back calculation of the parameters from the holding phase of the measured penetration history *h(t)* [Cheng et al. 2005; Vandamme and Ulm 2006; Jäger et al. 2007]. For identification of both elastic and viscous parameters, analytical solutions describing the penetration procedure are available [Sneddon 1965; Lee 1955; Radok 1957; Lee and Radok 1960; Hunter 1960; Graham 1965, 1967; Ting 1966, 1968] and employed for parameter identification.

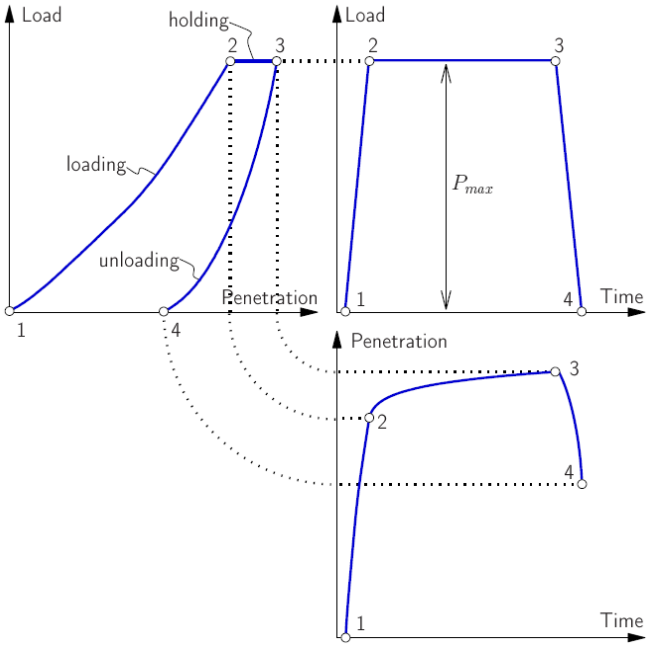

Figure 1-1 Load-penetration curve, load history, and penetration history for indentation test on material exhibiting elastic, viscous, and plastic material response

As regards identification of plastic parameters, on the other hand, no analytical solutions for plastic material behavior exist. Hence, numerical methods need to be applied for parameter identification. Such a numerical approach has been applied recently for the special case of conical indenter shapes [Pichler 2007], extracting so-called scaling relations for conical viscoelastic-cohesive indentation from numerical results.

In this line, the scaling-relation approach given in [Pichler 2007] is extended towards the case of spherical indenter shapes in this thesis. For this purpose, the elastic as well as elasto-plastic material response is studied by means of finite element analyses and compared (for the elastic case) to existing analytical solutions. These analytical solutions for spherical indentation into an elastic halfspace are presented in following section. Moreover, a dimensionless representation of the results is proposed. In Section 3, the employed finite element model and the chosen simulation parameters (tip radii and material parameters) are given. By comparing the elastic analytical and numerical indentation response (Subsection 4.1) first insight into the effect of underlying simplifications in the analytical solutions is gained. The results from elasto-plastic simulations are presented in dimensionless form in Subsection 4.2. In Section 5, the identification of plastic material parameters from instrumented indentation tests on the basis of the obtained numerical results is discussed. Furthermore, the onset of plastic deformation during elasto-plastic spherical penetration is identified from the numerical results. Finally, some concluding remarks close this thesis.

2 Analytical solutions for spherical penetration

According to the literature, there exist two analytical models to describe the contact between a sphere and an elastic halfspace:

1. According to Hertz, two elastic spheres are considered assuming that:
   a) the elastic limit is not passed,
   b) the contact area is significantly smaller than the radii R_1 [m] and R_2 [m] of the spheres, and that
   c) only normal stress acts at the contact surface.

   The relation between the contact force P [N] and the contact deformation h [m] is given by

$$P = K\ R^{0.5} h^{1.5}\,, \tag{2-1}$$

   where the contact curvature $\frac{1}{R}$ [1/m] and the contact modulus K [Pa] are defined as:

$$\frac{1}{R} = \frac{1}{R_1} + \frac{1}{R_2} \text{ and } K = \frac{4}{3}\left(\frac{1-\nu_1^{\,2}}{E_1} + \frac{1-\nu_2^{\,2}}{E_2}\right)^{-1} \tag{2-2) and (2-3}$$

   with R_1, ν_1 [-], E_1 [Pa] and R_2, ν_2 [-], E_2 [Pa] as the radius , Poisson's ratio, and Young's modulus of the two spheres, respectively.

   For the case of a rigid sphere (radius $R_1 = R$, Young's modulus $E_1 = \infty$) penetrating an elastic halfspace (radius $R_2 = \infty$, Young's modulus $E_2 = E$), the contact modulus *K* is obtained as

$$K = \frac{4}{3}\frac{E}{\left(1-\nu^2\right)} = \frac{4}{3}M\,, \tag{2-4}$$

   where *M* is the so-called indentation modulus. Inserting Equation (2-4) into Equation (2-3) gives the applied load *P* as a function of the penetration *h* for the Hertz solution as

$$P = \frac{4}{3}\frac{E}{\left(1-\upsilon^2\right)} R^{0.5} h^{1.5} . \qquad (2\text{-}5)$$

2. The so-called Sneddon solution [Sneddon 1965] describes the contact between an axisymmetric tip and an infinite elastic halfspace. Hereby, the tip shape is described by a smooth function *f(ρ)* (see Figure 2-1), where ρ is the radius of the axisymmetric tip. According to [Sneddon 1965], the penetration *h* [m] and the applied load *P* [N] are given by:

$$h = a \int_{\rho=0}^{a} \frac{f'(\rho)\cdot d\rho}{\sqrt{a^2-\rho^2}} \quad \text{and} \qquad P = 2\frac{E}{1-\upsilon^2} \int_{\rho=0}^{a} \frac{\rho^2 \cdot f'(\rho)\cdot d\rho}{\sqrt{a^2-\rho^2}}, \qquad (2\text{-}6) \text{ and } (2\text{-}7)$$

where *a* [m] is the radius of the projected contact area A_c [m^2], $f' = df/d\rho$, and E [Pa] and ν [-] are Young's modulus and Poisson's ratio, respectively.

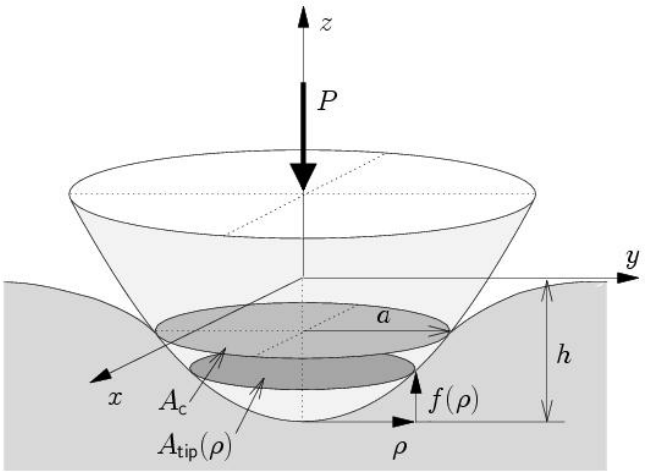

Figure 2-1 Contact between rigid axisymmetric indenter of shape *f(ρ)* and an infinite halfspace (*P* is the applied load, *h* is the penetration, and *a* is the contact radius)

In the case of spherical tips, the parameters C_0 and C_1 of the tip-shape function

$$f(\rho) = \frac{1}{2C_0}\left(\sqrt{C_1^2 + 4C_0\rho^2\pi} - C_1\right) \qquad (2\text{-}8)$$

are given by $C_0=-\pi$ [-] and $C_1=2R\pi$ [m], yielding

$$f(\rho) = R - \sqrt{R^2-\rho^2} . \qquad (2\text{-}9)$$

Specializing Equations (2-6) for the case of a spherical tip shape defined by the tip-shape function given in Equation (2-9), one gets

$$h = 0.5a\log\left(\frac{R+a}{R-a}\right) \text{ and} \tag{2-10}$$

$$P = \frac{E}{2(1-\upsilon^2)}\left[\left(a^2 + R^2\right)\log\left(\frac{R+a}{R-a}\right) - 2aR\right] \tag{2-11}$$

According to Equation (2-11), the penetration depth depends only on geometrical properties, such as the contact radius a and the tip radius R. The penetration load, on the other hand, is a function of a, R, and the mechanical properties of the elastic halfspace, represented by Young's modulus E and Poisson's ratio ν.

Figure 2-2 shows a comparison of the load-penetration curves obtained by the Hertz and the Sneddon solution, respectively. For small penetration depths, both solutions are in good agreement. For increasing penetration depths, the Hertz solution which is only valid for small penetrations leads to an underestimation of the penetration depth.

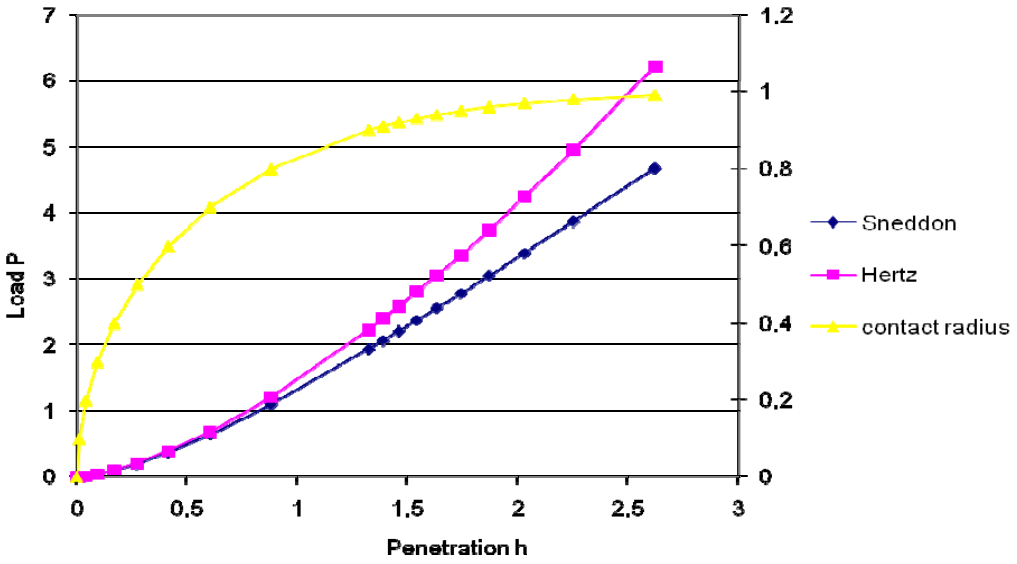

Figure 2-2 Load-penetration curve and increase of contact radius for penetration of spherical tip into elastic halfspace given by the Hertz and the Sneddon solution (R=1 m, E=1 Pa, ν=0.3)

In case of the spherical elastic indentation problem, the underlying problem is described by five physical quantities: the penetration load P [N], Young's modulus E [N/mm²], the radius of the spherical indenter R [mm], the penetration depth h [mm], and Poisson's ratio ν. Considering the Hertz

solution (see Equation (2-5)) and applying dimensional analysis gives the dimensionless variable Π_P as

$$\Pi_p = \frac{P}{Eh^{1.5}R^{0.5}} = \Pi_p\left(\upsilon, \Pi_h = \frac{h}{R}\right), \tag{2-12}$$

depending only on two dimensionless parameters, i.e., ν and $\Pi_h = \frac{h}{R}$.

Considering Equation (2-5) in Equation (2-12) leads to

$$\Pi_P^{Hertz} = \frac{4}{3\left(1-\upsilon^2\right)} = const., \tag{2-13}$$

with Π_P^{Hertz} being independent of Π_h (see Figure 2-3). As regards the Sneddon solution, $\Pi_P^{Sneddon}$ decreases continuously with increasing Π_h (see Figure 2-3). Figure 2-4 shows the influence of Poisson's ratio on $\Pi_P^{Sneddon}$, with lower values for $\Pi_P^{Sneddon}$ for decreasing ν.

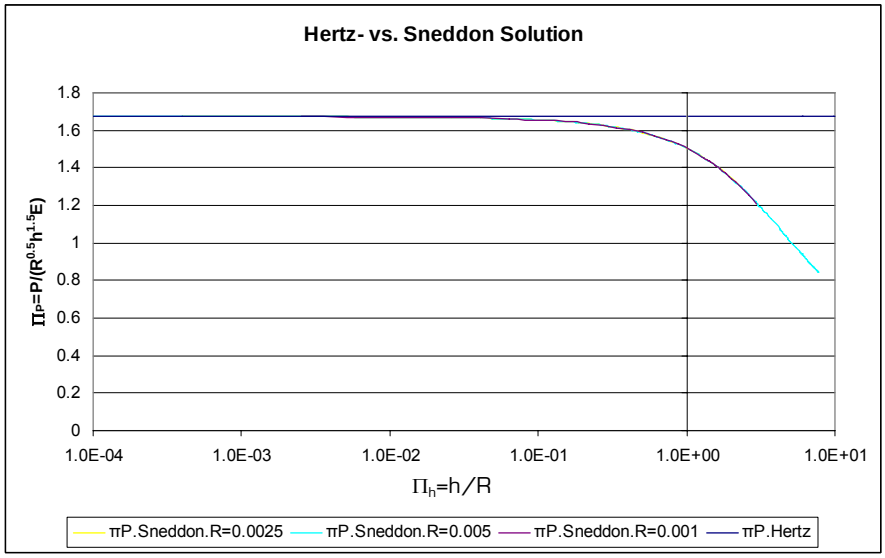

Figure 2-3 Comparison of Hertz and Sneddon solution (ν=0.45)

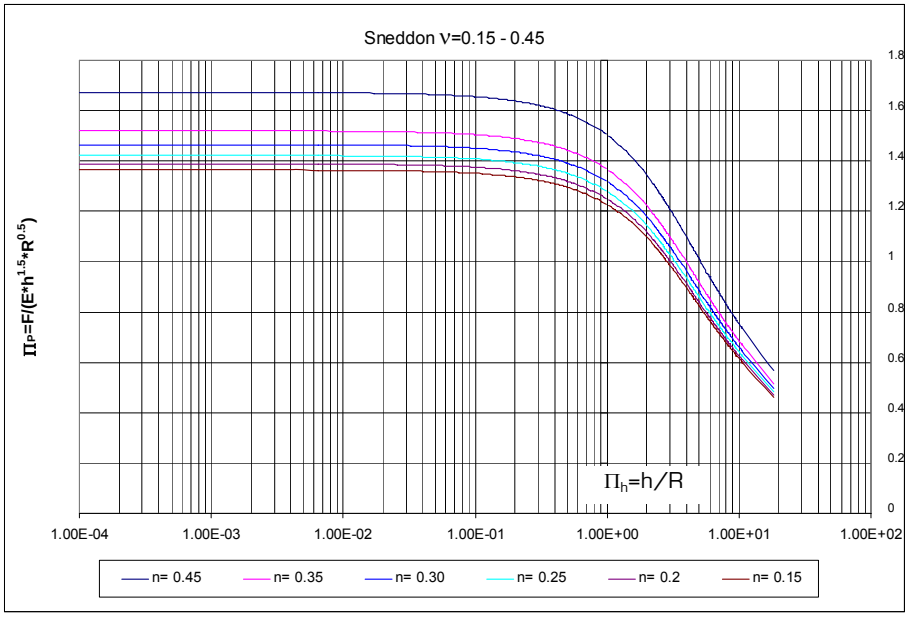

Figure 2-4 Sneddon solution for ν=0.15, 0.20, 0.25, 0.30, 0.35, and 0.45

When plastic deformation is taken into account, a third dimensionless variable is introduced, reading for the von Mises yield criterion $\Pi_c = \frac{c}{E}$, where c [N/mm²] is the deviatoric yield strength, giving the uniaxial yield strength as $\sqrt{3/2}c$. Thus, Π_P depends on three dimensionless parameters, reading

$$\Pi_p = \frac{P}{Eh^{1.5}R^{0.5}} = \Pi_p\left(\upsilon, \Pi_h = \frac{h}{R}, \Pi_c = \frac{c}{E}\right).$$

3 Numerical model and considered model parameters

3.1 Discretization

For the simulation of the indentation process, an axisymmetric model is employed (see Figure 3-1). Figure 3-2 shows the mesh refinement employed in the vicinity of the indenter tip.

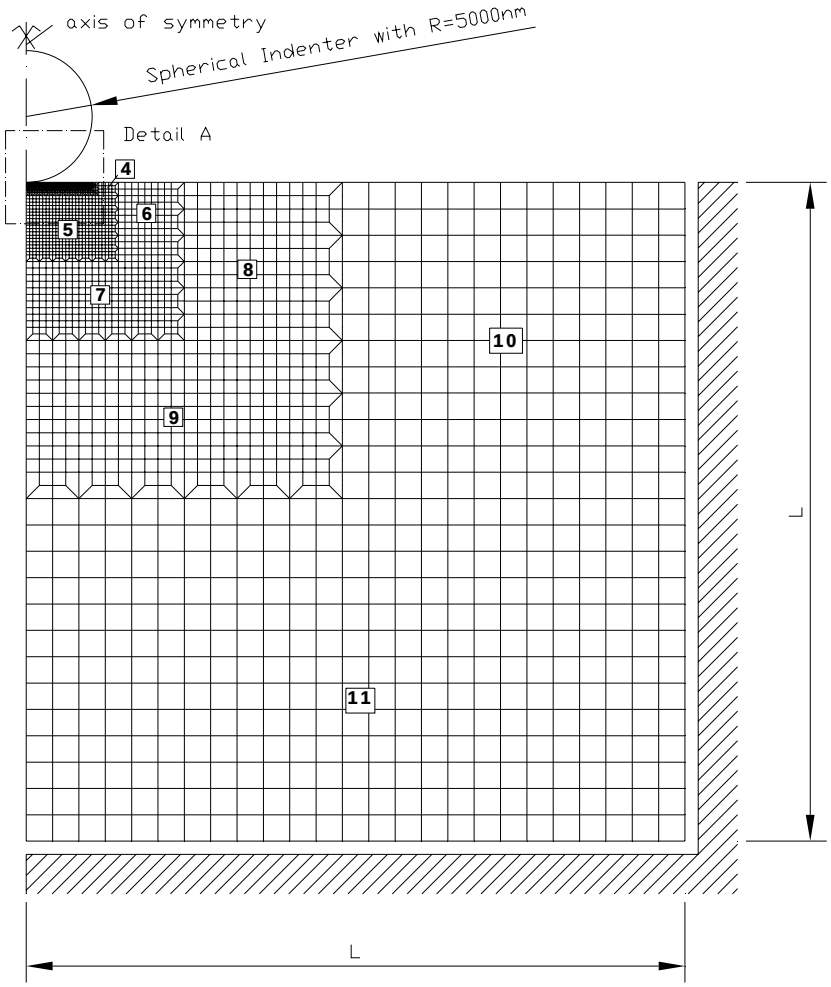

Figure **3-1** Numerical model and finite element mesh (L=50μm)

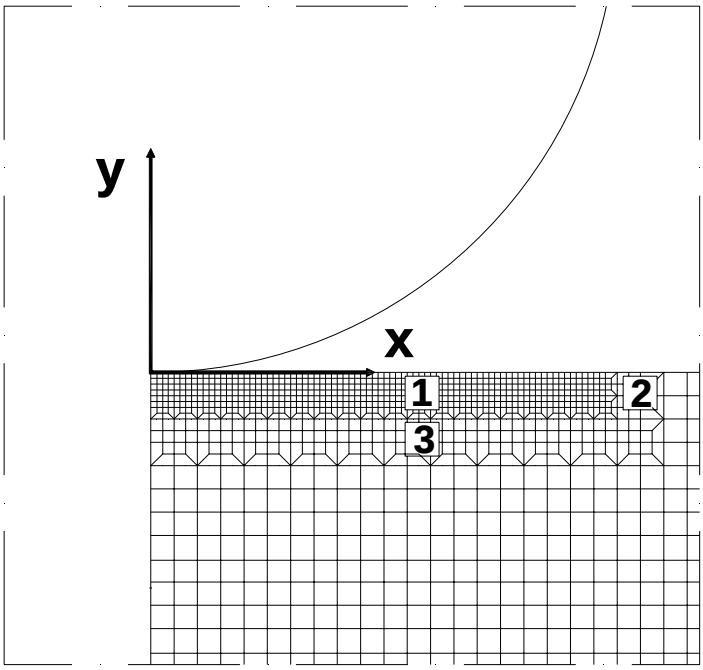

Figure 3-2 Finite-element mesh in the vicinity of the indenter tip

3.2 Simulation program

Numerical simulations are performed considering elastic as well as elasto-plastic material response. The elastic material behavior is described by Young's modulus E [N/mm²] and Poisson's ratio ν. In case of plastic material behavior, the deviatoric yield strength c [N/mm²] defines the elastic limit (von Mises yield criterion, ideally-plastic behavior).

For all simulations, three different radii of the spherical indenter are considered (see Table 3-2).

R [mm]	C1
0.001	0.00628
0.0025	0.01571
0.005	0.03142

Table 3-2 Considered indenter radius R and respective value C1

For the simulation considering elastic material response, Young's modulus and Poisson's ratio were varied according to Table 3-3.

E [N/mm²]	ν	G [N/mm²]	K [N/mm²]
11500	0.15	5000	5476
12000	0.15	5217	5714
12500	0.20	5208	6944
13000	0.20	5416	7222
13500	0.25	5400	9000
14500	0.25	5800	9666
80500	0.30	30961	67083
84000	0.30	32307	70000
87500	0.35	32407	97222
91000	0.35	33703	101111
94500	0.45	32586	315000
101500	0.45	35000	338333

Table 3-3 Considered parameters describing elastic behavior

Tables 3-4 to 3-7 contain Young's modulus *E*, yield strength *c*, Poisson's ratio ν, the c/E-ratio, shear modulus *G,* and bulk modulus *K* considered in the numerical simulations accounting for elasto-plastic material behavior.

E[N/mm²]	c[N/mm²]	c/E	ν	G[N/mm²]	K[N/mm²]
10000	50	0.005	0.45	3448	33333
10000	100	0.01	0.45	3448	33333
10000	250	0.025	0.45	3448	33333
10000	500	0.05	0.45	3448	33333
10000	1000	0.1	0.45	3448	33333
10000	2500	0.25	0.45	3448	33333
10000	5000	0.5	0.45	3448	33333
10000	7500	0.75	0.45	3448	33333
10000	10000	1	0.45	3448	33333
10000	50000	5	0.45	3448	33333
100000	10	0.0001	0.45	34482	333333
100000	50	0.0005	0.45	34482	333333
100000	100	0.001	0.45	34482	333333
100000	125	0.00125	0.45	34482	333333
100000	175	0.00175	0.45	34482	333333
100000	300	0.003	0.45	34482	333333
100000	500	0.005	0.45	34482	333333
100000	1000	0.01	0.45	34482	333333
100000	2500	0.025	0.45	34482	333333
100000	5000	0.05	0.45	34482	333333
100000	7500	0.075	0.45	34482	333333
100000	10000	0.1	0.45	34482	333333
100000	50000	0.5	0.45	34482	333333

Table 3-4 Considered parameter describing elasto-plastic behavior with ν=0.45

E[N/mm²]	c[N/mm²]	c/E	ν	G[N/mm²]	K[N/mm²]
10000	50	0.005	0.3	3846	8333
10000	500	0.05	0.3	3846	8333
10000	2500	0.25	0.3	3846	8333
25000	50	0.002	0.3	9615	20833
100000	50	0.0005	0.3	38461	83333
100000	100	0.001	0.3	38461	83333
100000	1000	0.01	0.3	38461	83333
100000	1500	0.015	0.3	38461	83333
100000	2500	0.025	0.3	38461	83333
100000	7500	0.075	0.3	38461	83333
100000	50000	0.5	0.3	38461	83333

Table 3-5 Considered parameter describing elasto-plastic behavior with ν=0.30

E[N/mm²]	c[N/mm²]	c/E	ν	G[N/mm²]	K[N/mm²]
10000	500	0.05	0.15	4347	4761
10000	1000	0.1	0.15	4347	4761
10000	2500	0.25	0.15	4347	4761
25000	50	0.002	0.15	10869	11904
25000	100	0.004	0.15	10869	11904
25000	500	0.02	0.15	10869	11904
25000	1000	0.04	0.15	10869	11904
25000	5000	0.2	0.15	10869	11904
100000	50	0.0005	0.15	43478	47619
100000	100	0.001	0.15	43478	47619
100000	500	0.005	0.15	43478	47619
100000	1000	0.01	0.15	43478	47619
100000	50000	0.5	0.15	43478	47619

Table 3-6 Considered parameter describing elasto-plastic behavior with ν=0.15

E[N/mm²]	c[N/mm²]	c/E	ν	G[N/mm²]	K[N/mm²]
10000	100	0.01	0	5000	3333
10000	250	0.025	0	5000	3333
10000	500	0.05	0	5000	3333
10000	750	0.075	0	5000	3333
10000	1000	0.1	0	5000	3333
10000	1250	0.125	0	5000	3333
10000	1500	0.15	0	5000	3333
10000	2000	0.2	0	5000	3333
10000	2500	0.25	0	5000	3333
10000	3000	0.3	0	5000	3333
10000	4000	0.4	0	5000	3333
10000	5000	0.5	0	5000	3333
10000	7500	0.75	0	5000	3333

Table 3-7 Considered parameter describing elasto-plastic behavior with ν=0.0

4 Presentation of results

4.1 Results from elastic FEM simulations

Elastic FEM simulations are performed considering five different Poisson's ratios and two Young's moduli, and three sphere radii as specified in Subsection 3.2. The numerical results and the respective analytical solutions are given in Figures 4-1 to 4-6. The results are plotted in dimensionless form, using the dimensionless parameters Π_p and $\Pi_h = \frac{h}{R}$.

According to Figures 4-1 to 4-6, the dimensionless parameter Π_p is independent of Young's modulus and the tip radius, depending only on Poisson's ratio as already observed for the Hertz solution. The oscillating shape of the curves stems from the discrete nature of the FEM, resulting in an increasing stiffness as a new node of the FE-mesh gets in contact with the tip.

Comparing the numerical results with the analytical solutions, two major differences can be found:

1. The numerical results give a higher dimensionless parameter Π_p than the analytical solution. This deviation is found for all considered Poisson's ratios.
2. Whereas the numerical results are more or less parallel to the analytical solution for high Poisson's ratios (nearly incompressible material), an increasing deviation is found for decreasing values of Poisson's ratio. The slope of the numerical solution for Π_P increases with decreasing Poisson's ratio. The shape of the analytical solution, on the other hand, is the same for all considered Poisson's ratios.

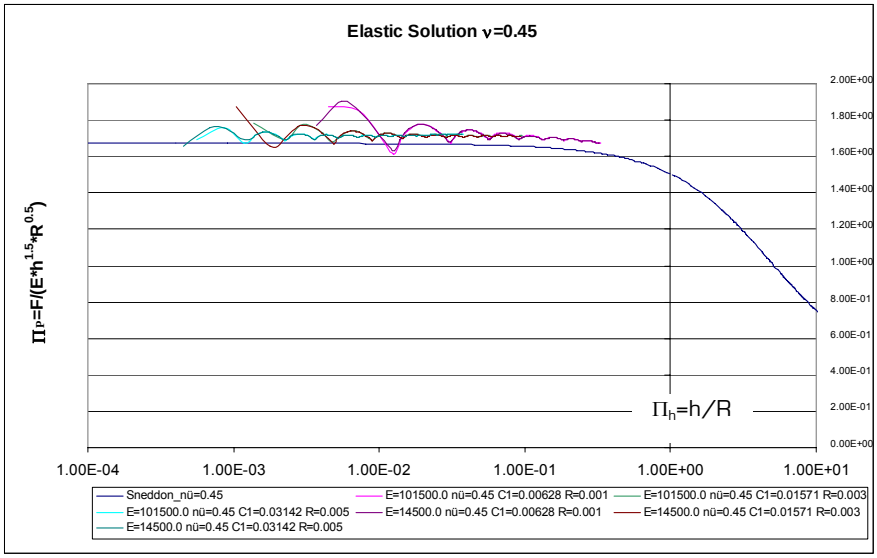

Figure 4-1 Numerical results vs. Sneddon solution considering elastic behavior (ν=0.45)

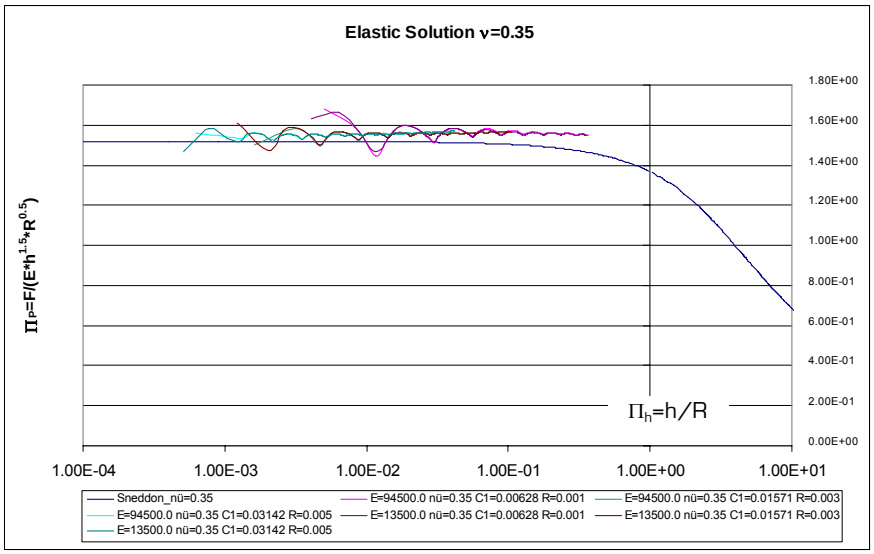

Figure 4-2 Numerical results vs. Sneddon solution considering elastic behavior (ν=0.35)

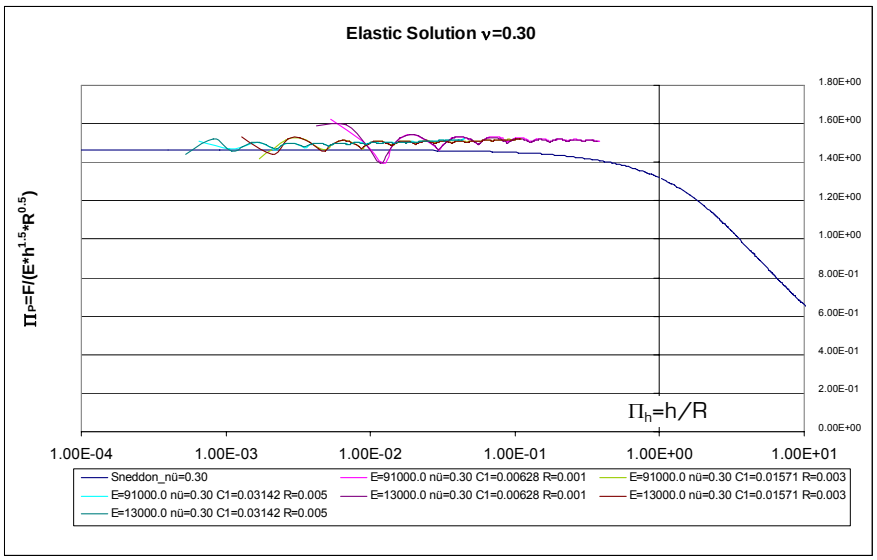

Figure 4-3 Numerical results vs. Sneddon solution considering elastic behavior (ν=0.30)

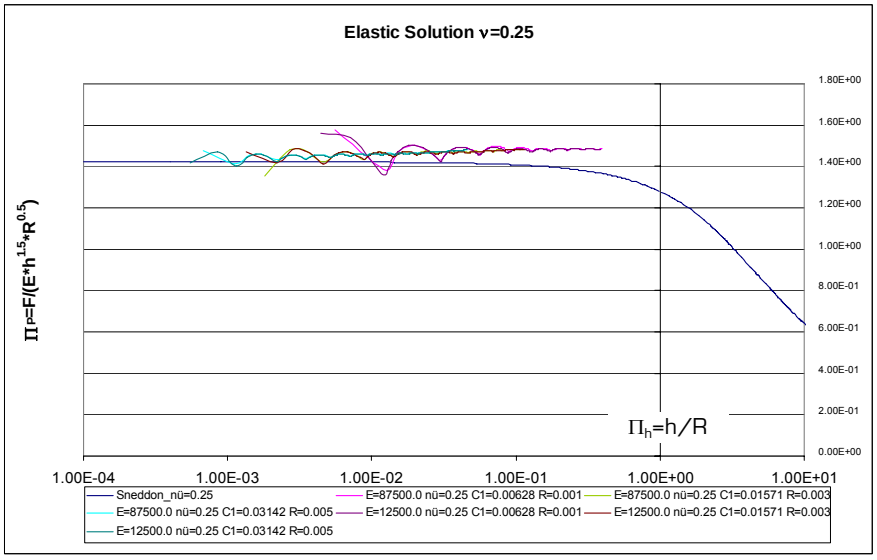

Figure 4-4 Numerical results vs. Sneddon solution considering elastic behavior (ν=0.25)

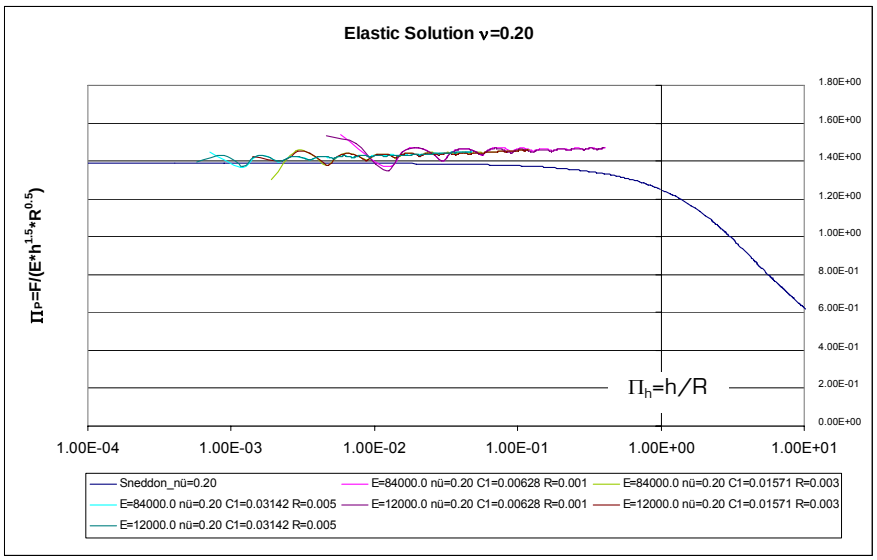

Figure 4-5 Numerical results vs. Sneddon solution considering elastic behavior (ν=0.20)

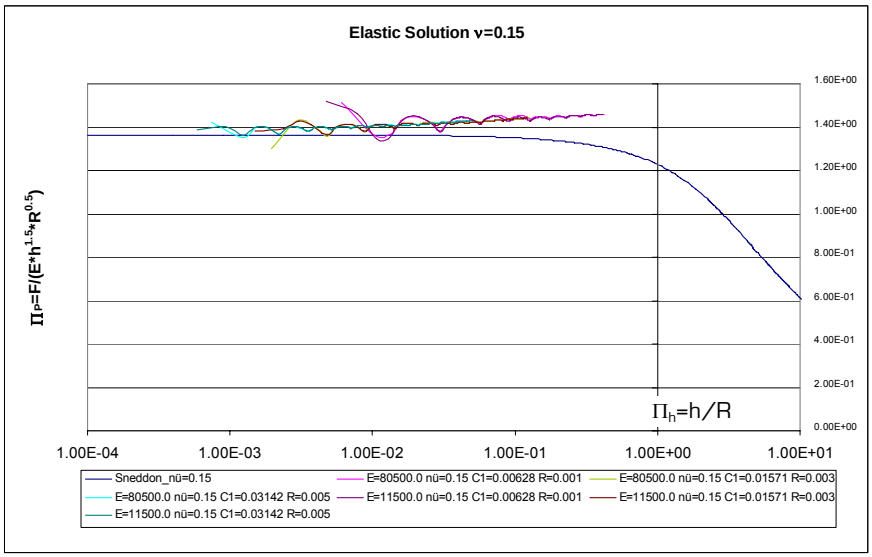

Figure 4-6 Numerical results vs. Sneddon solution considering elastic behavior (ν=0.15)

In order to account for the observed deviation between the numerical results and the analytical Sneddon solution, the Sneddon solution is modified by a two-step procedure. First, the numerical results are approximated by:

$$\tilde{\Pi}_P = k_\nu \log(h/R) + d_\nu \qquad (4\text{-}1)$$

with k_ν as the slope in the logarithmic scale and d_ν as value of $\tilde{\Pi}_P$ at $\Pi_h = 1$.

Figures 4-7 to 4-12 show the approximation function $\tilde{\Pi}_P$ (red continuous line, fit performed within $0 < \Pi_h < 0.1$) for the considered Poisson's ratios. The corresponding values for k_ν and d_ν are given in Table 4-1.

Poisson ratio ν	k_ν	d_ν
0.15	0.033	1.47
0.2	0.028	1.48
0.25	0.023	1.51
0.3	0.019	1.54
0.35	0.014	1.58
0.45	0.000	1.72

Table 4-1 k_ν and d_ν for considered Poisson's ratio

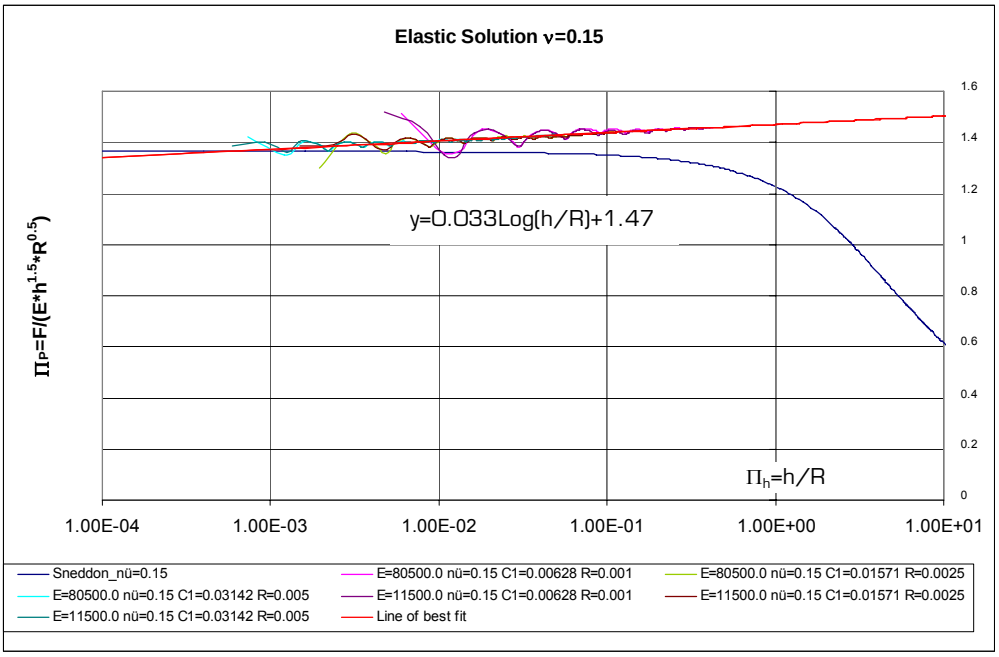

Figure 4-7 Approximation of numerical results for ν=0.15 and indenter radii 0.001, 0.0025, and 0.005

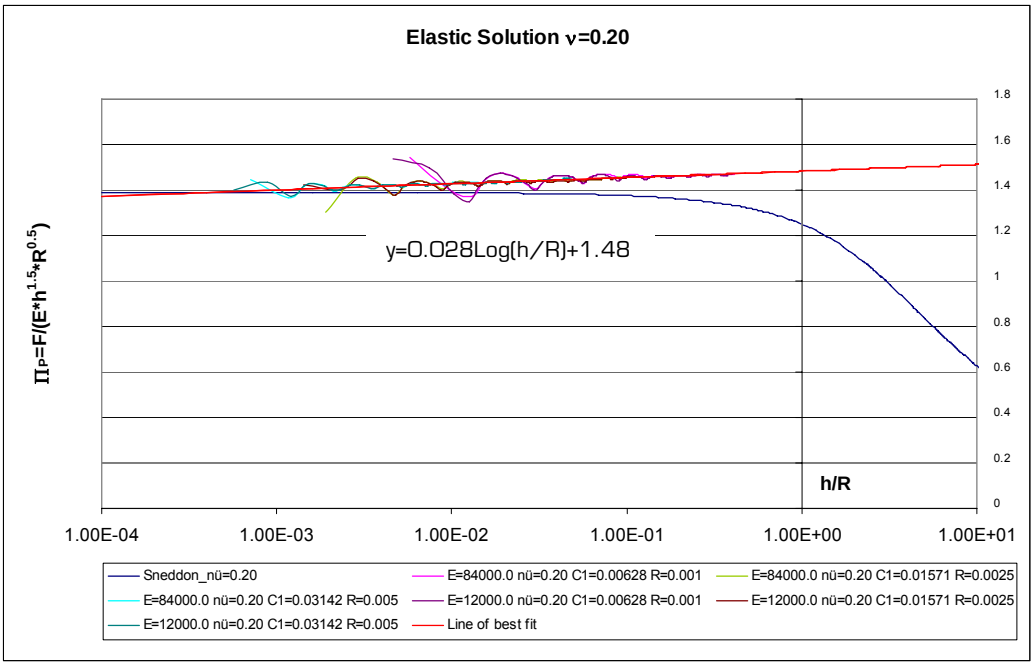

Figure 4-8 Approximation of numerical results for ν=0.20 and indenter radii 0.001, 0.0025, and 0.005

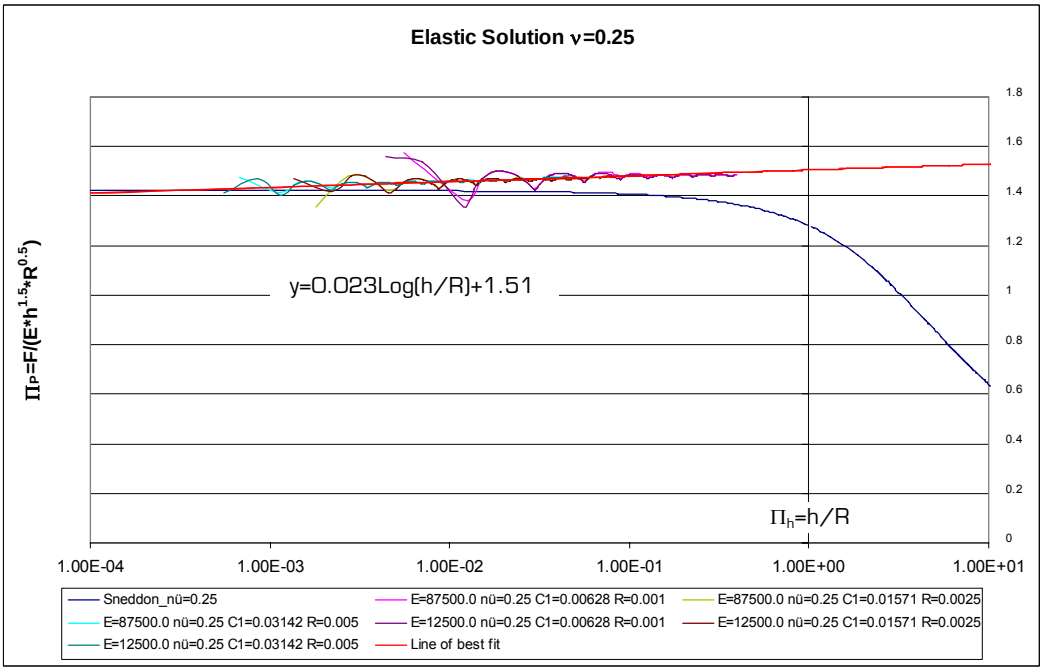

Figure 4-9 Approximation of numerical results for ν=0.25 and indenter radii 0.001, 0.0025, and 0.005

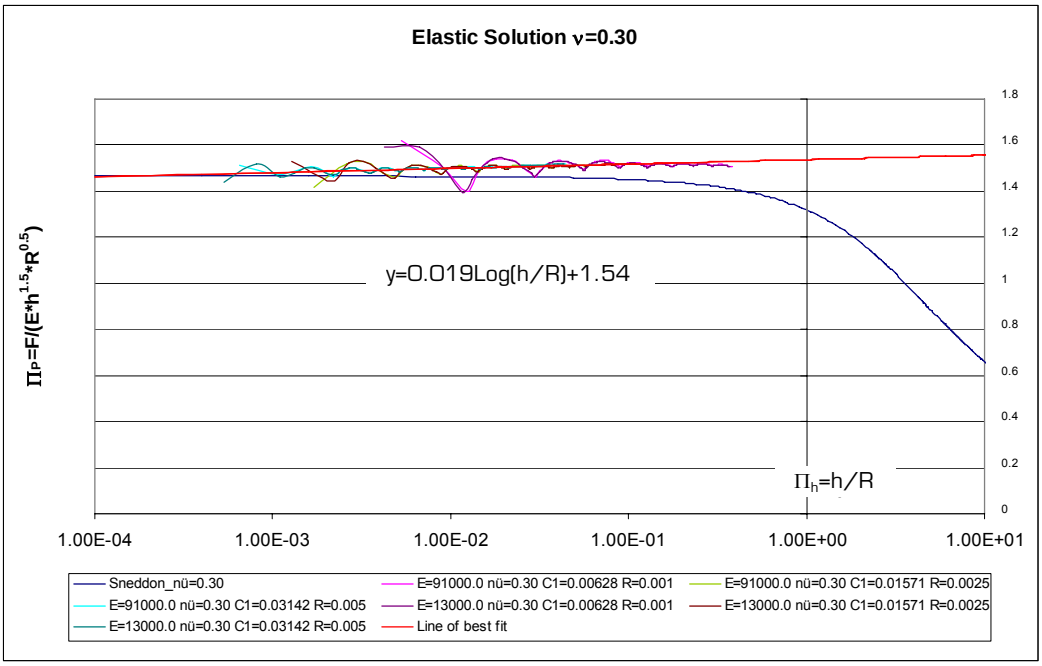

Figure 4-10 Approximation of numerical results for ν=0.30 and indenter radii 0.001, 0.0025, and 0.005

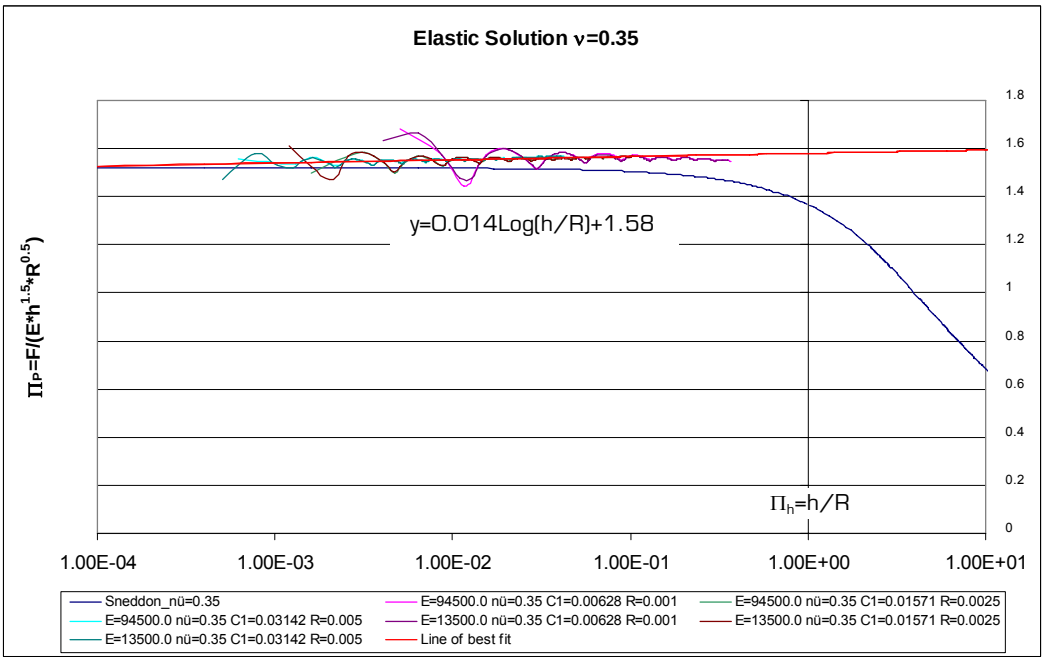

Figure 4-11 Approximation of numerical results for ν=0.35 and indenter radii 0.001, 0.0025, and 0.005

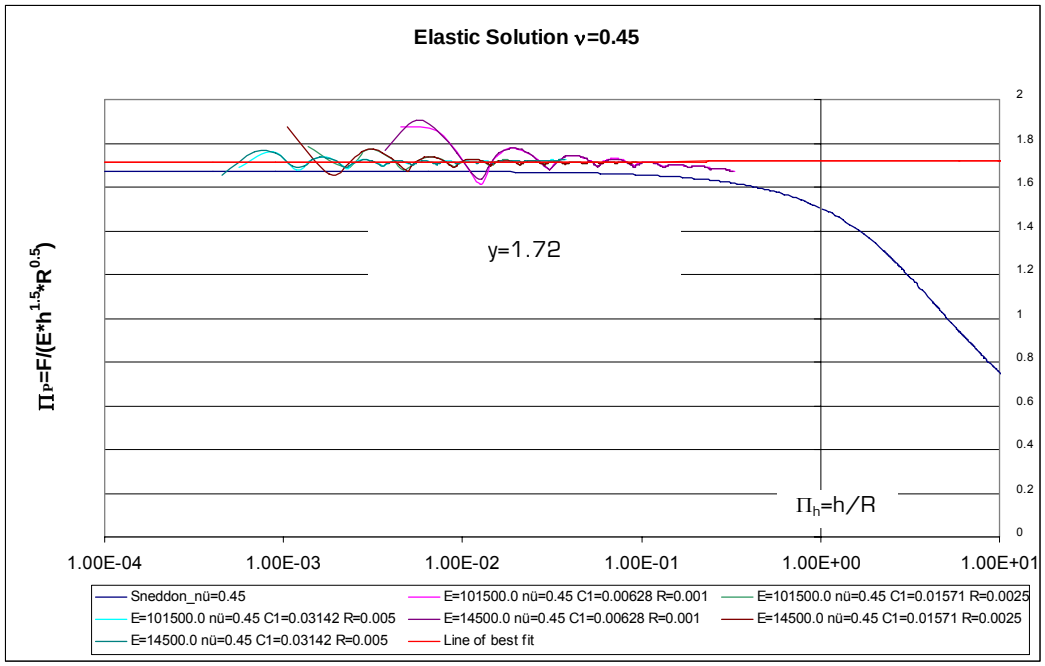

Figure 4-12 Approximation of numerical results for ν=0.45 and indenter radii 0.001, 0.0025, and 0.005

Secondly, the Sneddon solution is shifted towards the obtained approximation functions introducing the parameter β,defined by [1]

$$\beta = \frac{\tilde{\Pi}_P(\Pi_h = 0.01)}{\Pi_{P,Sneddon}(\Pi_h = 0.01)}. \qquad (4\text{-}2)$$

The computed values of β for the different Poisson's ratios are listed in Table 4-2.

Poisson ratio ν	$\Pi_{p,Sneddon}$(h/R=0.01) (Sneddon)	$\tilde{\Pi}_P$ (h/R=0.01) (approximation)	BETA-Factor
0.15	1.363	1.404	1.030
0.20	1.388	1.427	1.028
0.25	1.421	1.458	1.026
0.30	1.464	1.499	1.024
0.35	1.518	1.553	1.023
0.45	1.670	1.715	1.027

Table 4-2 BETA-Factor considered Poisson's ratios

[1] In Equation (4-2) Π_h=h/R=1% refers to moderate values for the penetration, being well-suited for the so-far considered elastic material response.

Finally, β and k_ν are employed for modifying the Sneddon solution, now reading

$$\Pi_{P.scaled\_Sneddon}(\Pi_h,\nu)=\Pi_{P.Sneddon}(\Pi_h,\nu)+\Pi_{P.Sneddon}(\Pi_h=0.01,\nu)\cdot\left[\beta(\nu)-1\right]+k_\nu(\nu)\cdot\log\left(\frac{\Pi_h}{0.01}\right) \qquad (4\text{-}3)$$

Figures 4-13 to 4-18 show a comparison of the modified Sneddon solution (green continuous line) with the results from numerical simulations for different Poisson's ratios.

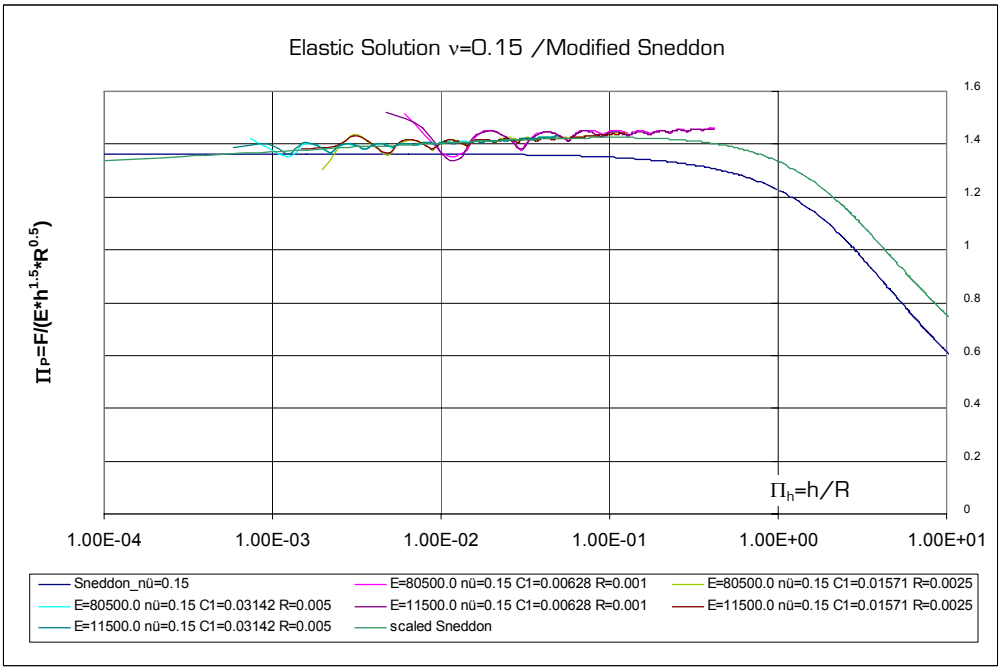

Figure 4-13 Modified Sneddon solution compared with the numerical results for Poisson's ratio of 0.15

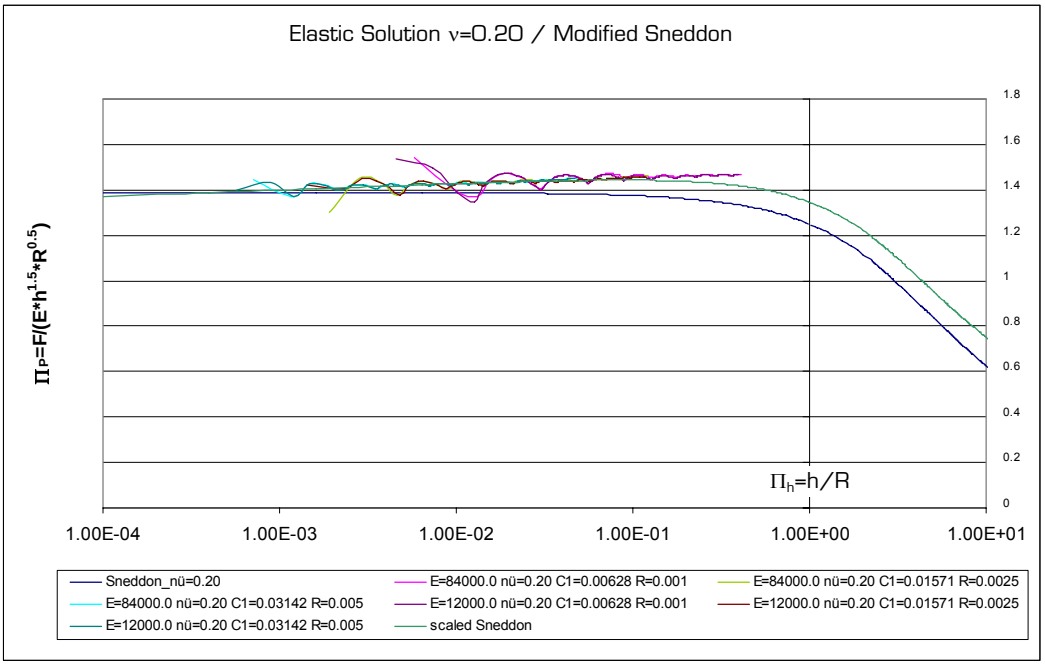

Figure 4-14 Modified Sneddon solution compared with the numerical results for Poisson's ratio of 0.20

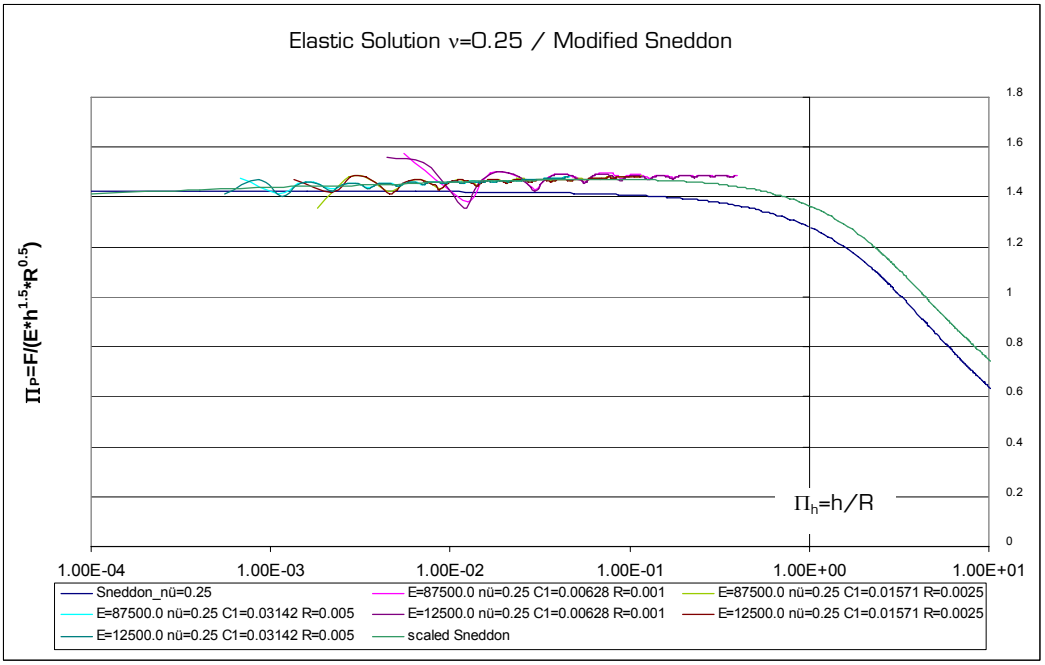

Figure 4-15 Modified Sneddon solution compared with the numerical results for Poisson's ratio of 0.25

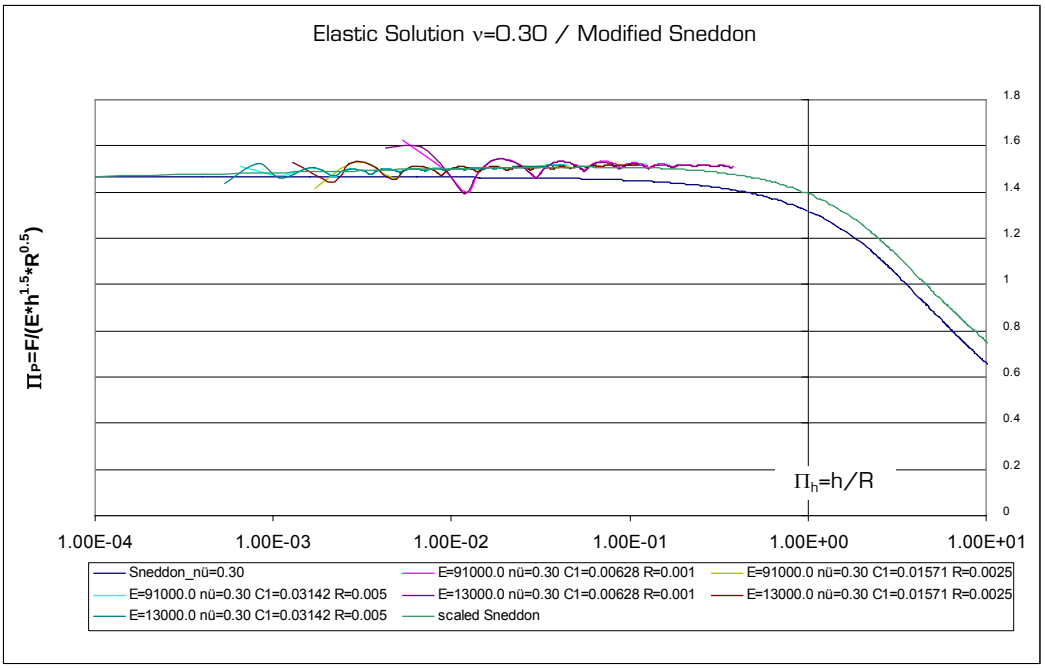

Figure 4-16 Modified Sneddon solution compared with the numerical results for Poisson's ratio of 0.30

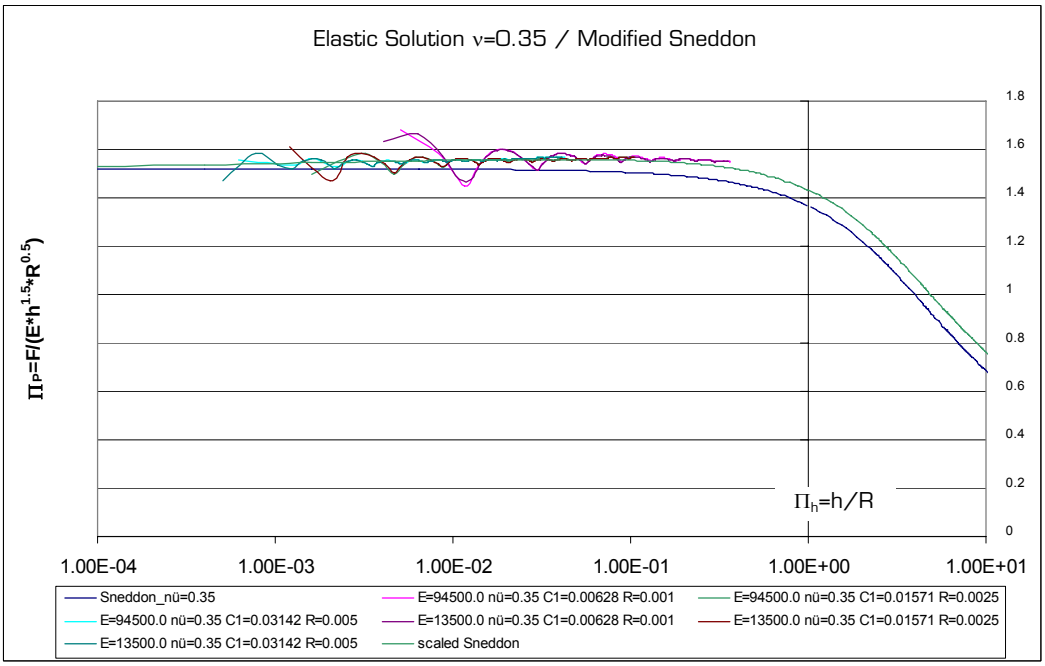

Figure 4-17 Modified Sneddon solution compared with the numerical results for Poisson's ratio of 0.35

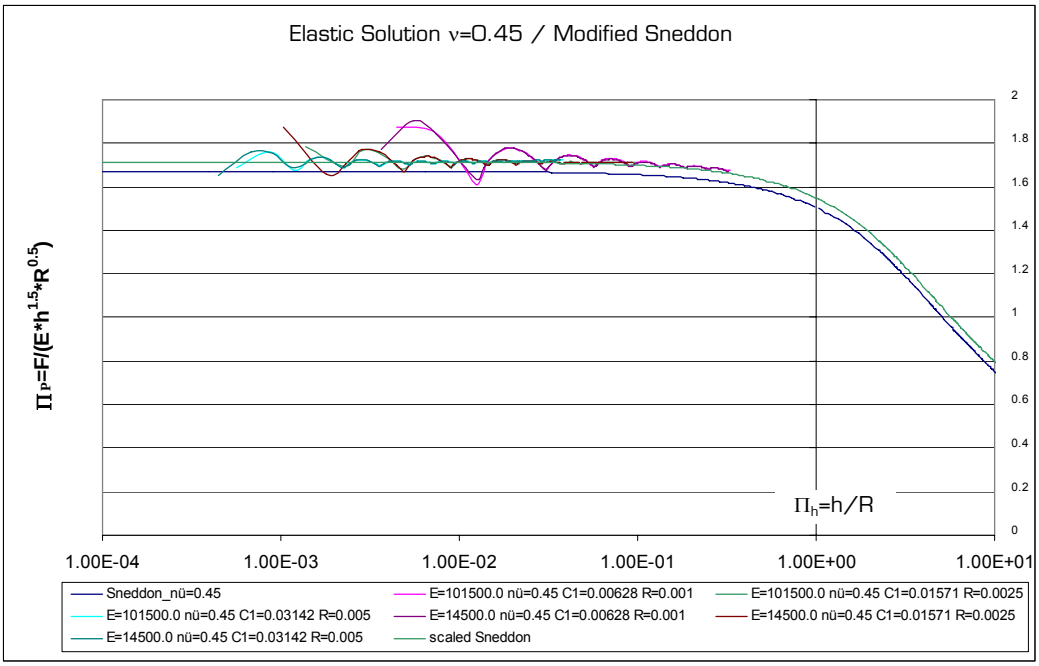

Figure 4-18 Modified Sneddon solution compared with the numerical results for Poisson's ratio of 0.45

4.2 Results from elasto-plastic FEM simulation

In case of spherical penetration into an elasto-plastic material, the amount of plastic deformation depends on

1. the resistance of the material to plastic deformation, i.e., the deviatoric yield strength *c* for materials described by the von Mises yield criterion,
2. the radius of the tip, influencing the pressure distribution,and
3. the maximum applied load.

Figures 4-19 to 4-21, showing load-penetration histories obtained from FEM simulations, illustrate the aforementioned influence of yield strength and tip radius on the penetration history. The simulations are performed for a Poisson's ratio of 0.45, a Young's modulus of 100000 N/mm^2, for three tip radii (0.005, 0.0025 and 0.001 mm), and three different values for the yield strength, giving c/E values of 100, 0.1, and 0.007.

In case of high c/E ratios (see Figure 4-19 for c/E=100), the loading and the unloading path coincide for all three tip radii, indicating elastic material behavior. For a c/E-ratio of 0.1 and a tip radius of 0.001 m (Figure 4-20), on the other hand, the loading and unloading paths are different and plastic deformation remains after unloading. For increasing tip radii (R=0.0025 mm),

the amount of plastic deformation decreases, with elastic material behavior indicated for a tip radius of 0.005 mm. When the c/E-ratio is further decreased to a value of 0.007 (Figure 4-21), the resulting stress exceeds the yield strength and plastic deformation is found for all considered tip radii.
Figures 4-19 to 4-21 highlight the influence of material and tip parameters on the amount of plastic deformation, depending on the combination of maximum load, tip radius and yield strength.
Figures 4-22 and 4-23 show the distribution of the vertical plastic strain component, ε_y^{pl}, at maximum load and after unloading (see Figure 4-20 for corresponding load-penetration history).

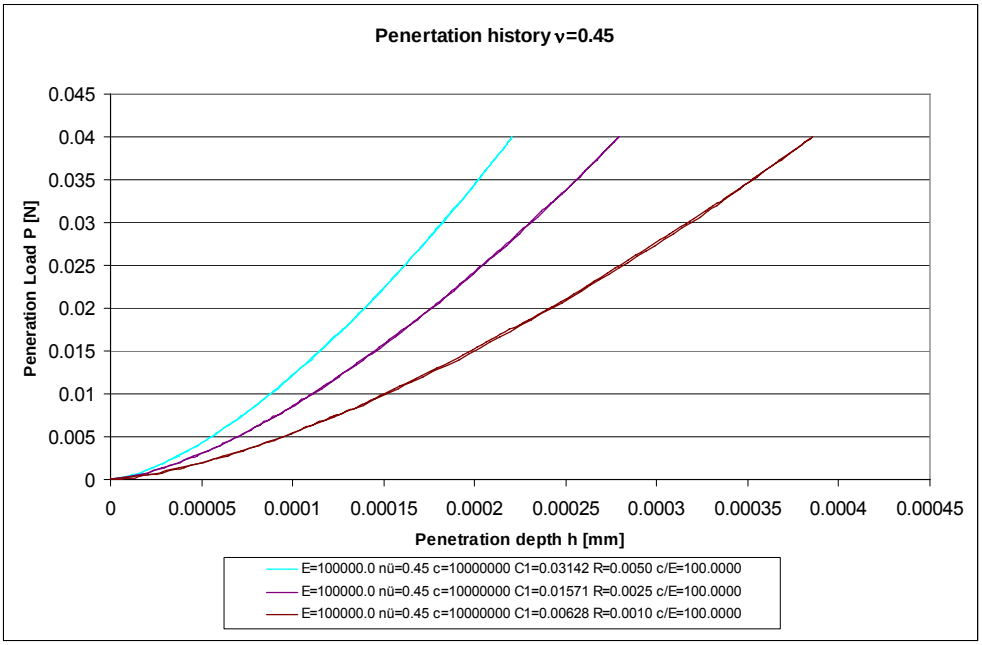

Figure 4-19 Load-penetration history from FEM simulation with c/E=100 for three different tip radii (R=0.005/0.0025/0.001 mm, ν=0.45, P_{max}=0.04 N)

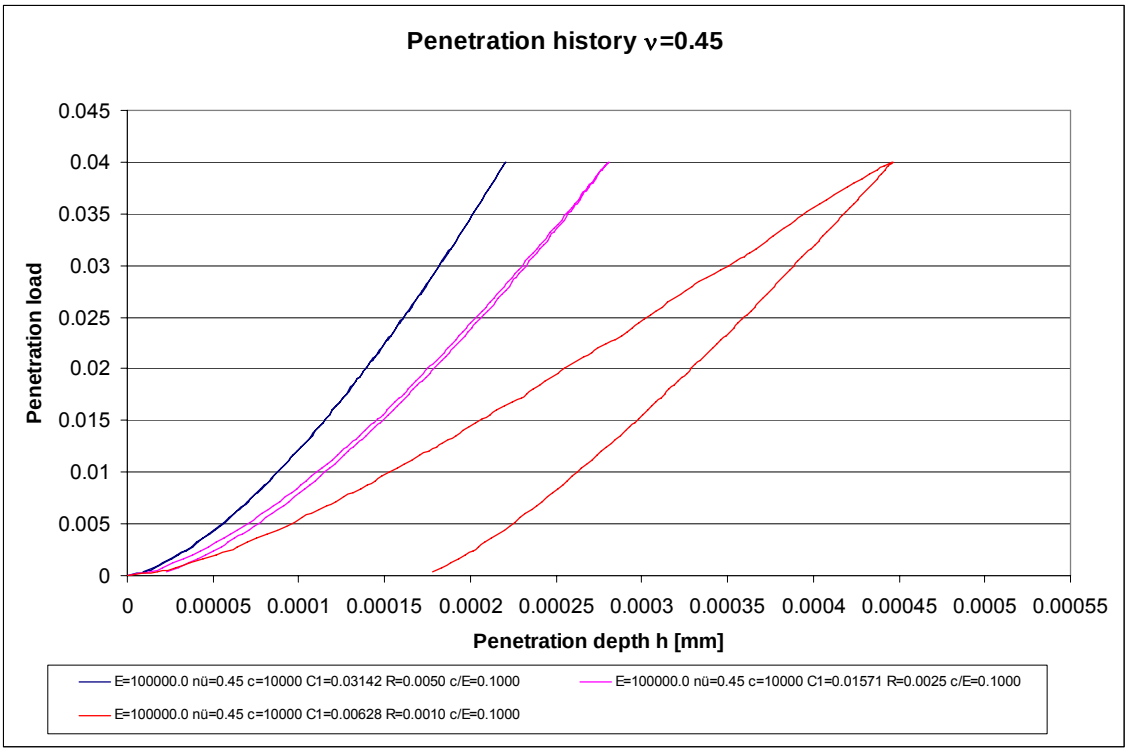

Figure 4-20 Load-penetration history from FEM simulation with c/E=0.10 for three different tip radii (R=0.005/0.0025/0.001 mm, ν=0.45, P_{max}=0.04 N)

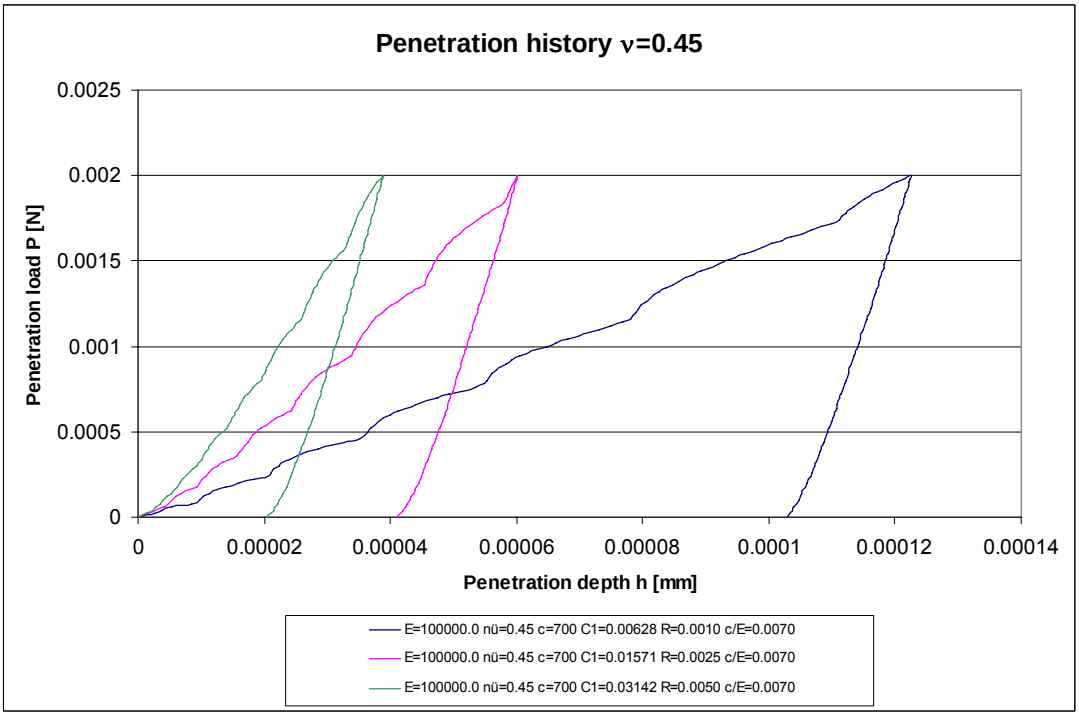

Figure 4-21 Load-penetration history from FEM simulation with c/E=0.007 for three different tip radii (R=0.005/0.0025/0.001 mm, ν=0.45, P_{max}=0.002 N)

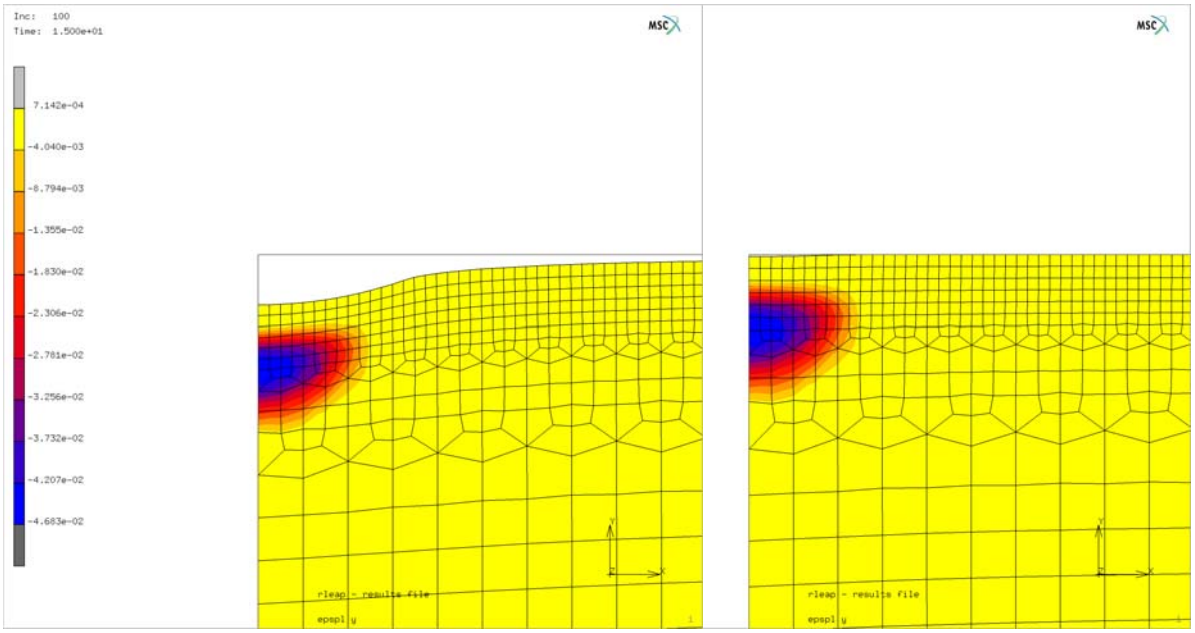

Figure 4-22 Distribution of vertical plastic strain component, at (a) maximum load and (b) after unloading for tip radius of R=0.0025 mm and Poisson's ratio of 0.45 (c/E=0.1)

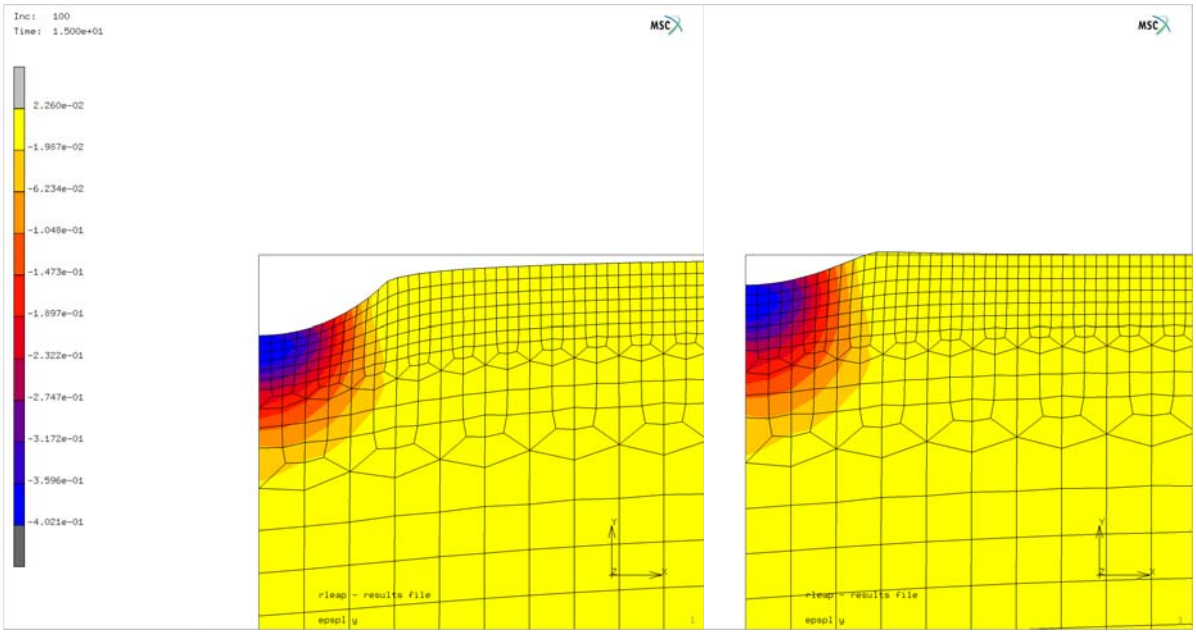

Figure 4-23 Distribution of vertical plastic strain component, at (a) maximum load and (b) after unloading for tip radius of R=0.0025 mm and Poisson's ratio of 0.45 (c/E=0.1)

As already mentioned in Subsection 2.3, the physical problem of spherical penetration into an elasto-plastic material can be described by the dimensionless parameter Π_P which depends on three dimensionless

parameters, i.e., Poisson's ratio (ν), the ratio between penetration depth and tip radius (Π_h), and the ratio between yield strength and Young's modulus (Π_c). Figure 4-24 shows numerical results, considering three different tip radii and two values for c and E giving a constant c/E-ratio, together with the analytical Sneddon solution for the elastic case (blue solid curve). The oscillation of the curves stems from the discrete nature of the FE model. Every kink corresponds to a surface node of the discretized material halfspace getting into contact with the rigid spherical indenter. The numerical analyses show that:

1. Π_P does not depend on the selected tip radius for a constant c/E-ratio
2. Π_P does not depend on the values of c and E as long as the respective c/E-ratio is constant, and
3. In case plastic deformation occurs, Π_P starts to decrease below the respective value of Π_p of the elastic solution.

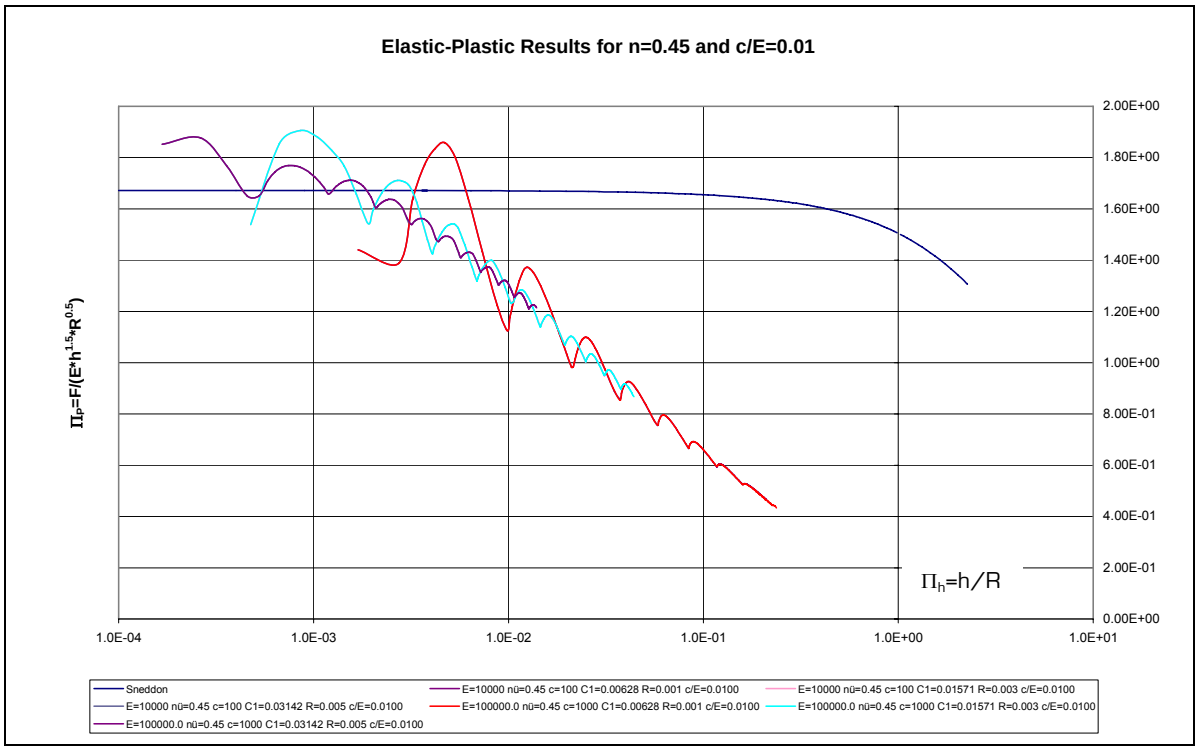

Figure 4-24 Numerical results from FE analysis of spherical penetration into elasto-plastic material considering different tip radii and values for yield strength c and Young's modulus E (with c/E-ratio=constant) compared with analytical elastic Sneddon solution

The elasto-plastic simulations are carried out for the parameter set given in Subsection 3.2. Three indenter radii (0.005 mm, 0.0025 mm, and 0.001 mm) and four Poisson's ratios (0.45, 0.30, 0.15, and 0.0) were considered in this study. The values for the deviatoric yield strength and Young's modulus are varied in order to cover a wide range of c/E-ratios. The investigated c/E-ratios are listed in Table 4-3 for each Poisson's ratio.

ν=0.45	ν=0.30	ν=0.15	ν=0.0
0.0001	0.0005	0.0005	0.01
0.0005	0.001	0.001	0.025
0.001	0.002	0.002	0.05
0.00125	0.005	0.004	0.075
0.00175	0.01	0.005	0.1
0.003	0.025	0.01	0.125
0.005	0.05	0.02	0.15
0.01	0.075	0.04	0.2
0.025	0.15	0.05	0.25
0.05	0.25	0.1	0.3
0.075	0.5	0.2	0.4
0.1		0.25	0.5
0.25		0.5	0.75
0.5			
0.75			
1			
5			

Table 4-3 c/E-ratios considered in the numerical simulations for different Poisson's ratios

Figures 4-25 to 4-36 show the obtained numerical results. For each Poisson's ratio, three figures are presented showing

a) the numerical results (oscillating curves),
b) the numerical results together with a smoothed curve for each c/E-ratio, and
c) the smoothed curves without the original numerical results.

In order to compare the numerical results with the analytical elastic solution, $\Pi_P^{Sneddon}$ (blue continuous line) is plotted in each figure.

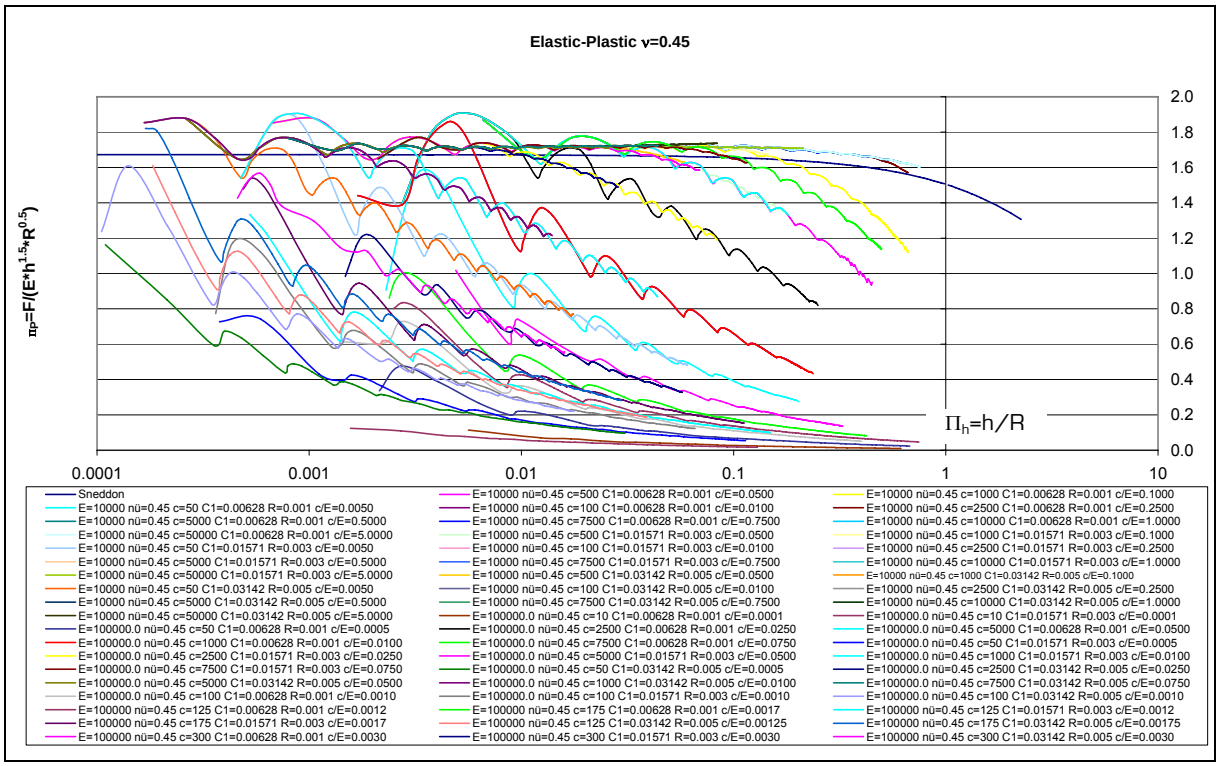

Figure 4-25 Dimensionless plot of numerical simulation results for elastic-plastic material for ν=0.45 and different c/E-ratios

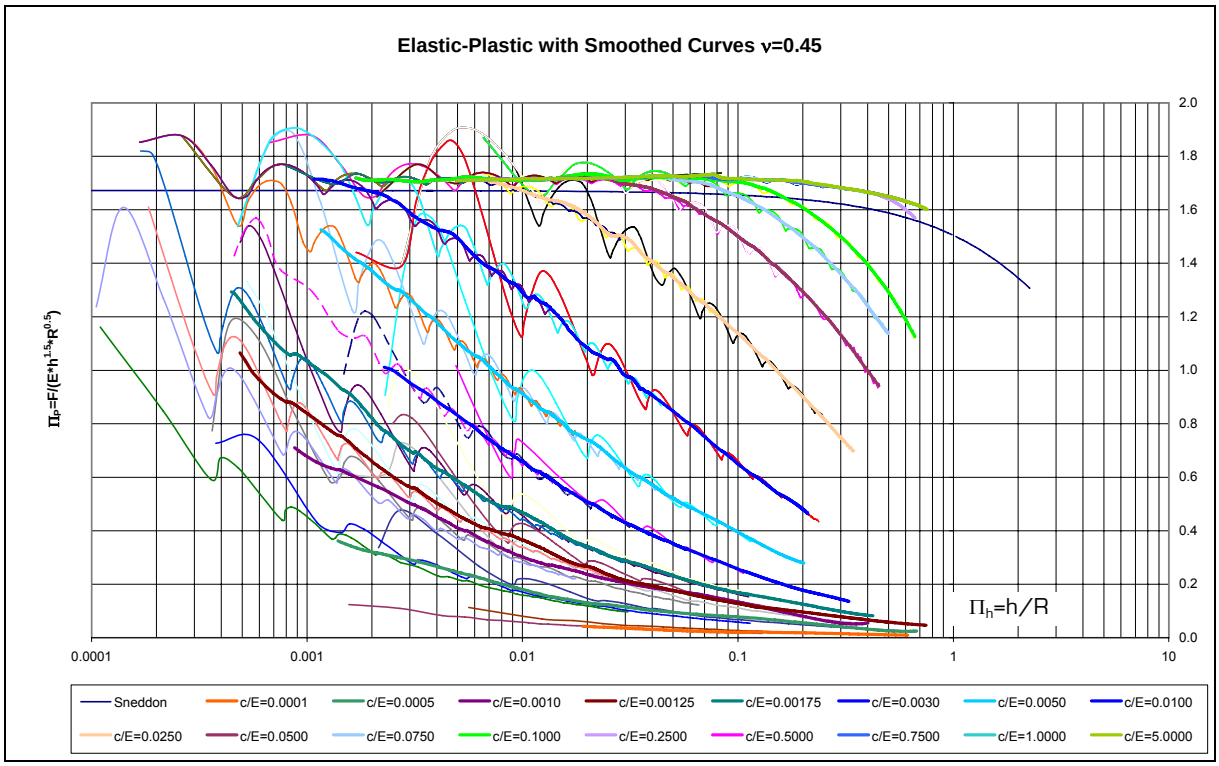

Figure 4-26 Dimensionless plot of smoothed and original numerical results for elastic-plastic material for ν=0.45 and different c/E-ratios

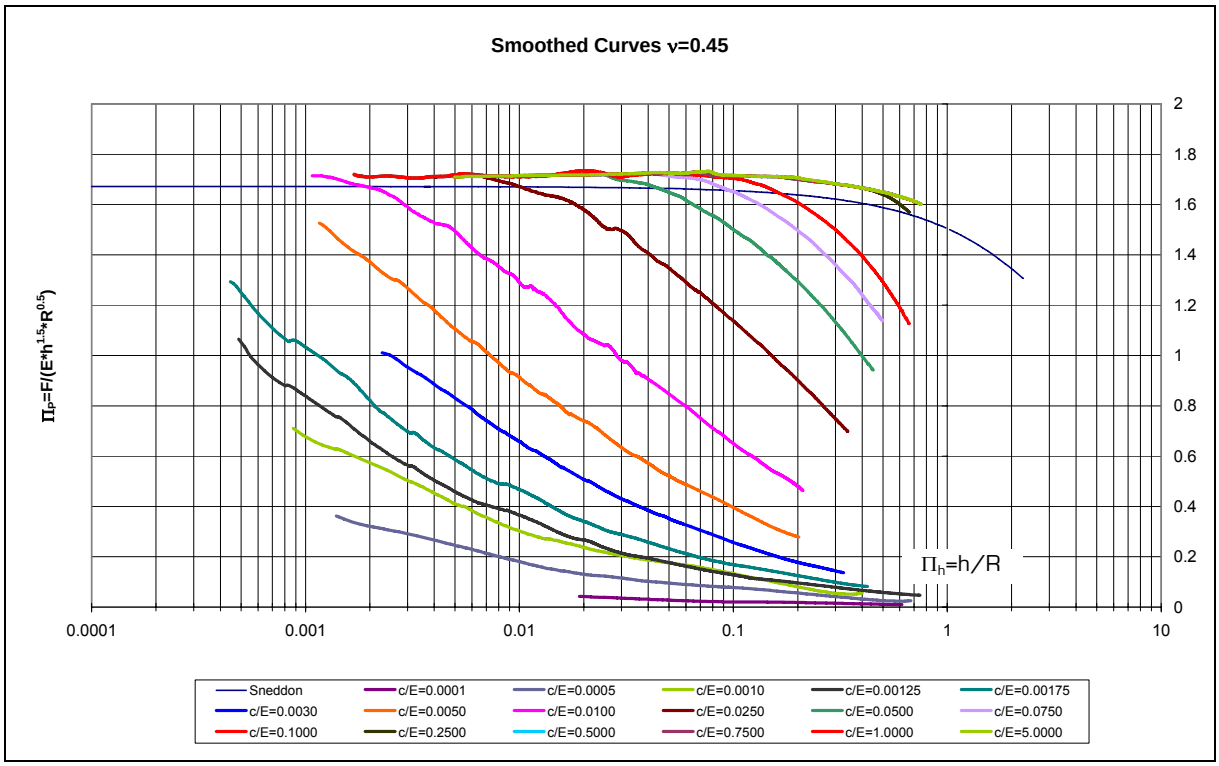

Figure 4-27 Dimensionless plot of smoothed numerical results for elastic-plastic material for ν=0.45 and different c/E-ratios

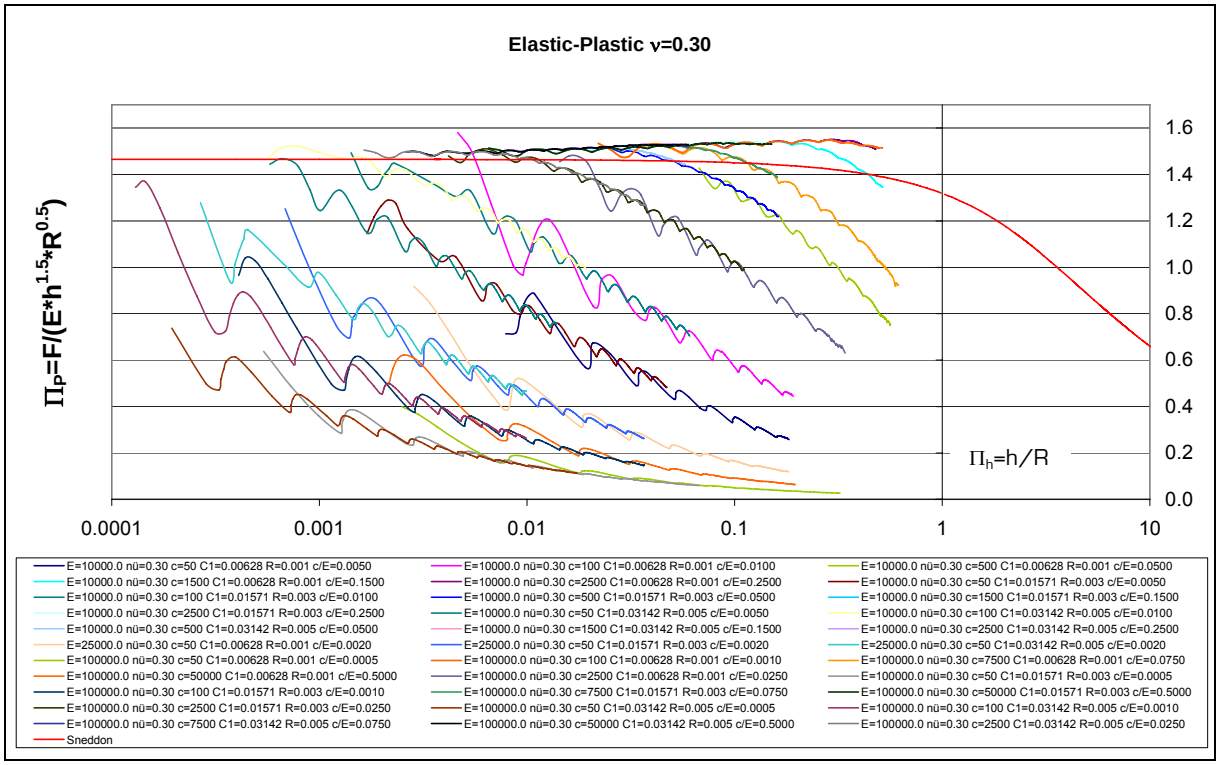

Figure 4-28 Dimensionless plot of numerical simulation results for elastic-plastic material for ν=0.30 and different c/E-ratios

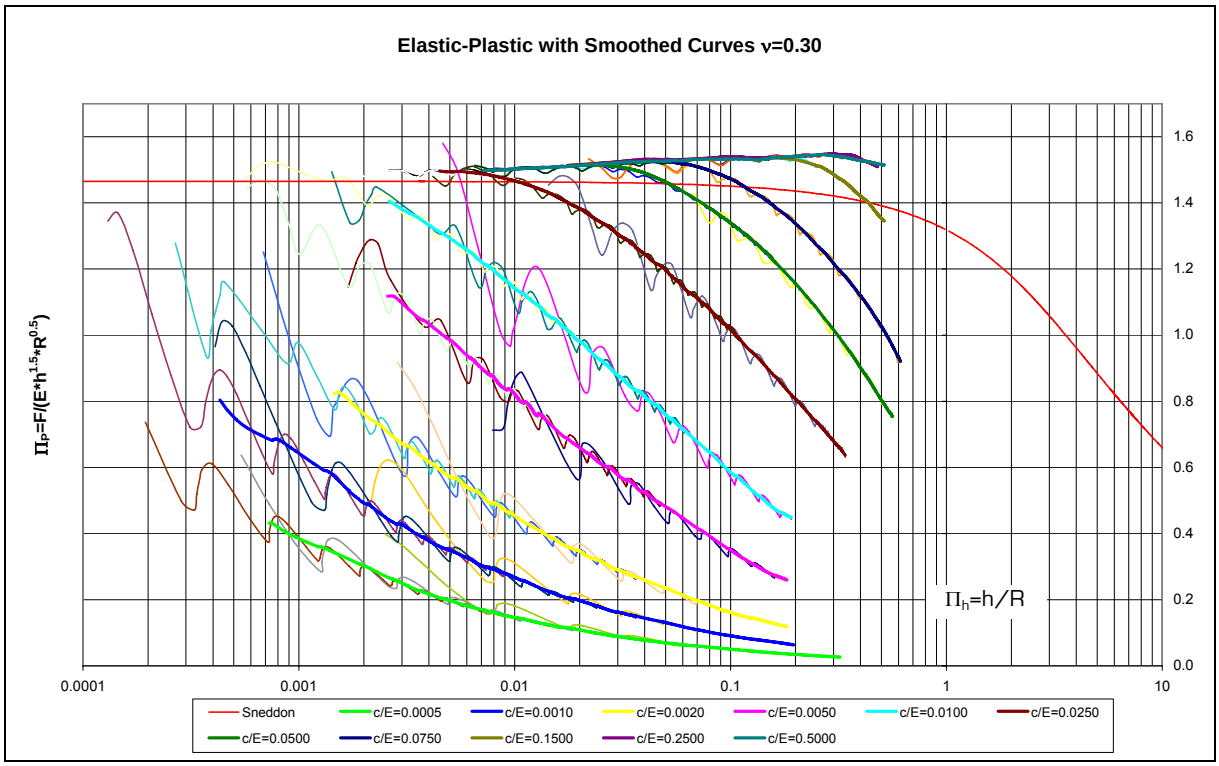

Figure 4-29 Dimensionless plot of smoothed and original numerical results for elastic-plastic material for ν=0.30 and different c/E-ratios

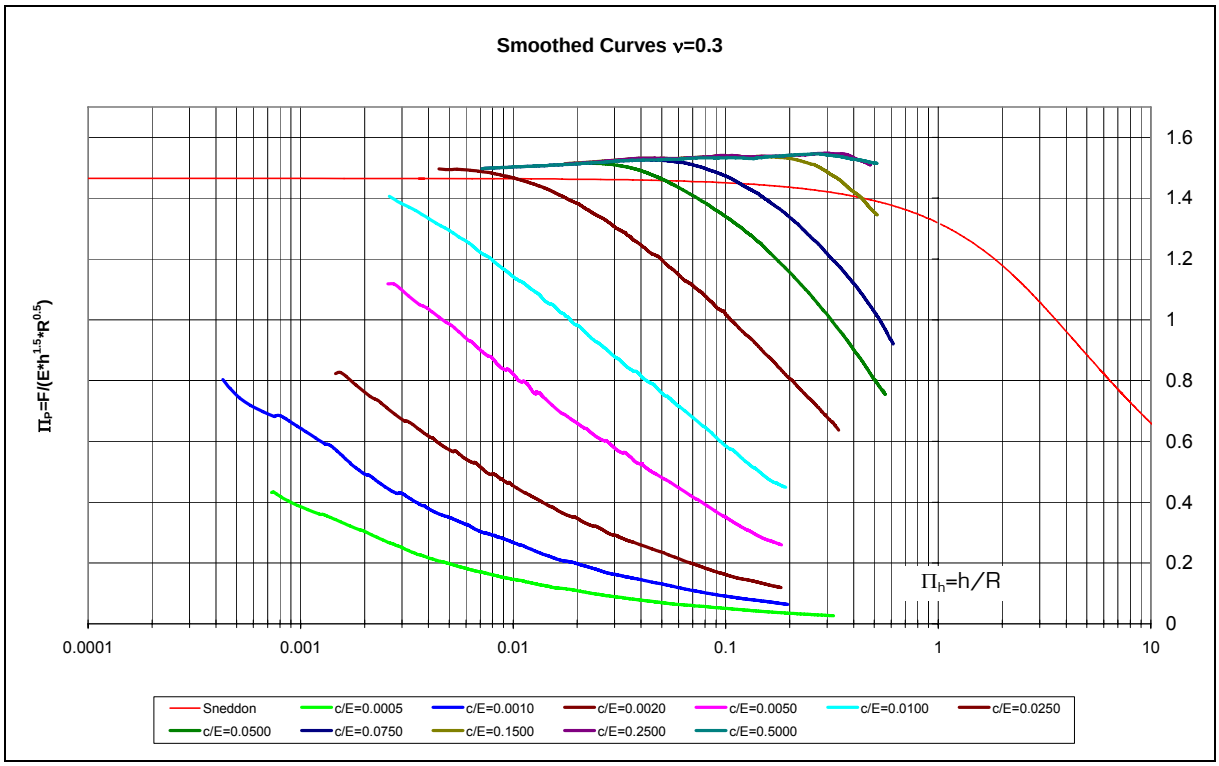

Figure 4-30 Dimensionless plot of smoothed numerical results for elastic-plastic material for ν=0.30 and different c/E-ratios

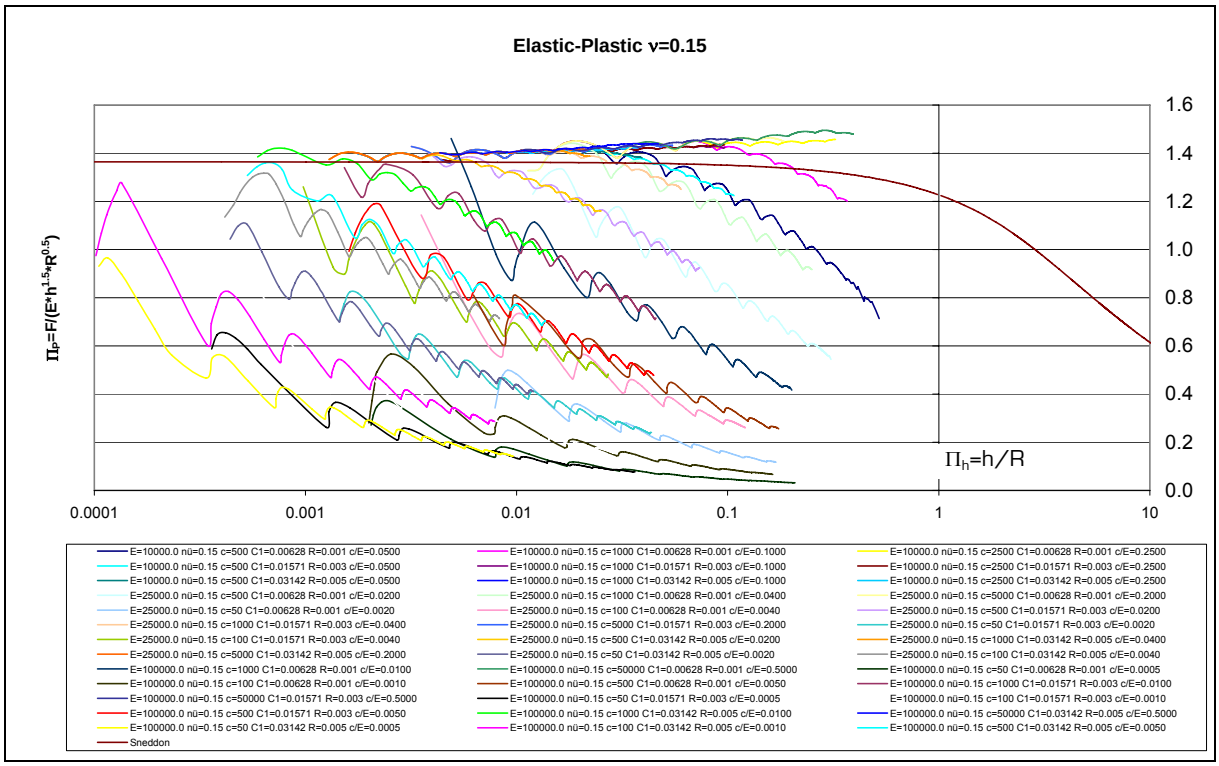

Figure 4-31 Dimensionless plot of numerical simulation results for elastic-plastic material for ν=0.15 and different c/E-ratios

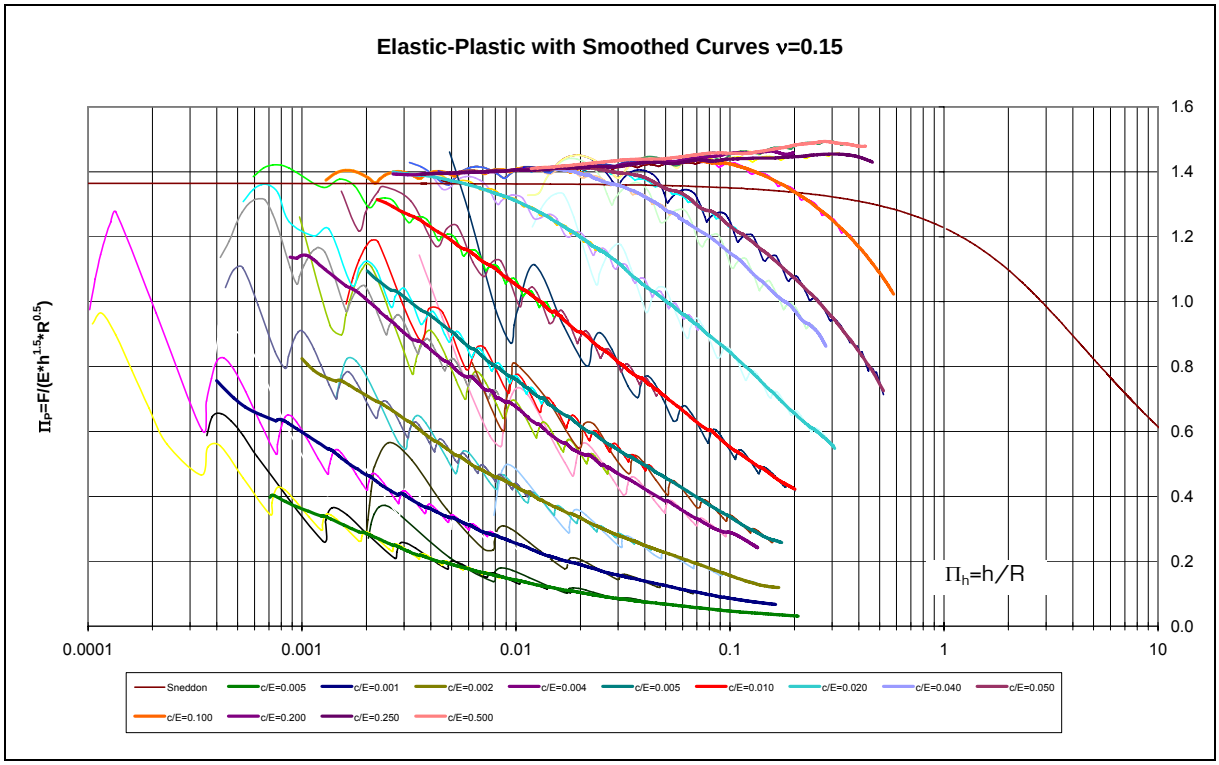

Figure 4-32 Dimensionless plot of smoothed and original numerical results for elastic-plastic material for ν=0.15 and different c/E-ratios

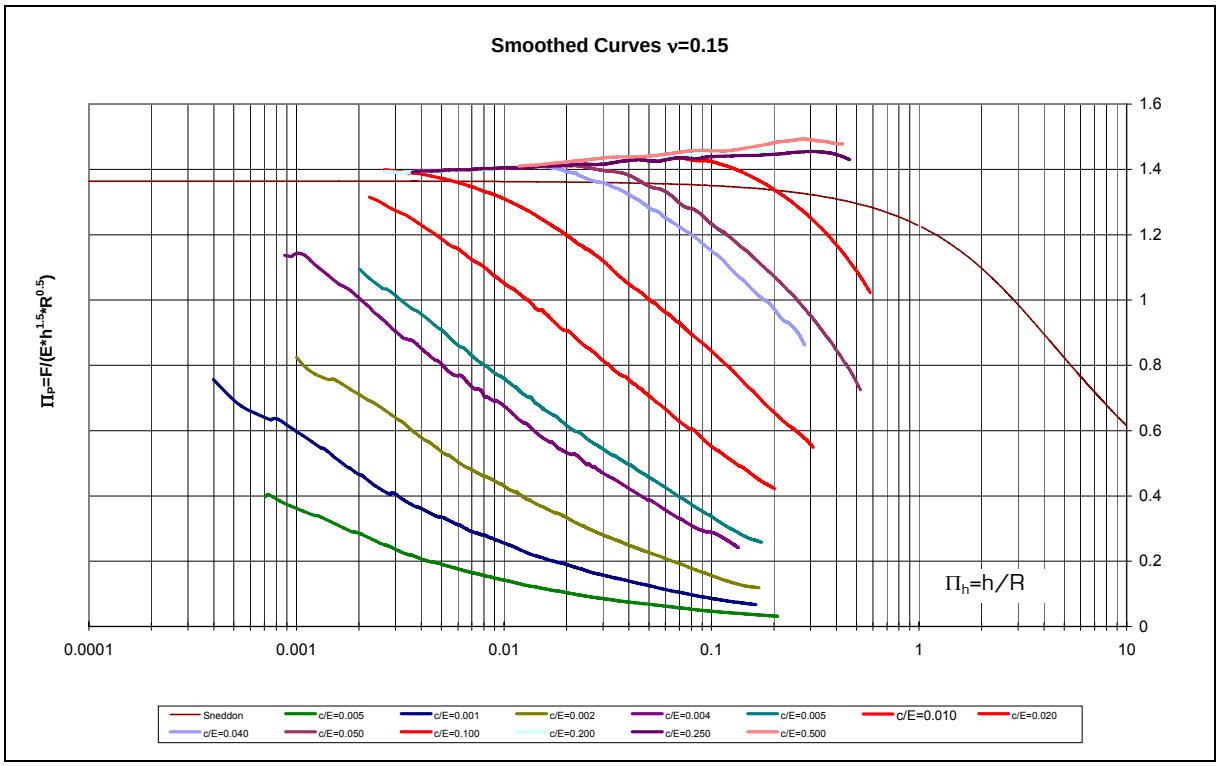

Figure 4-33 Dimensionless plot of smoothed numerical results for elastic-plastic material for ν=0.15 and different c/E-ratios

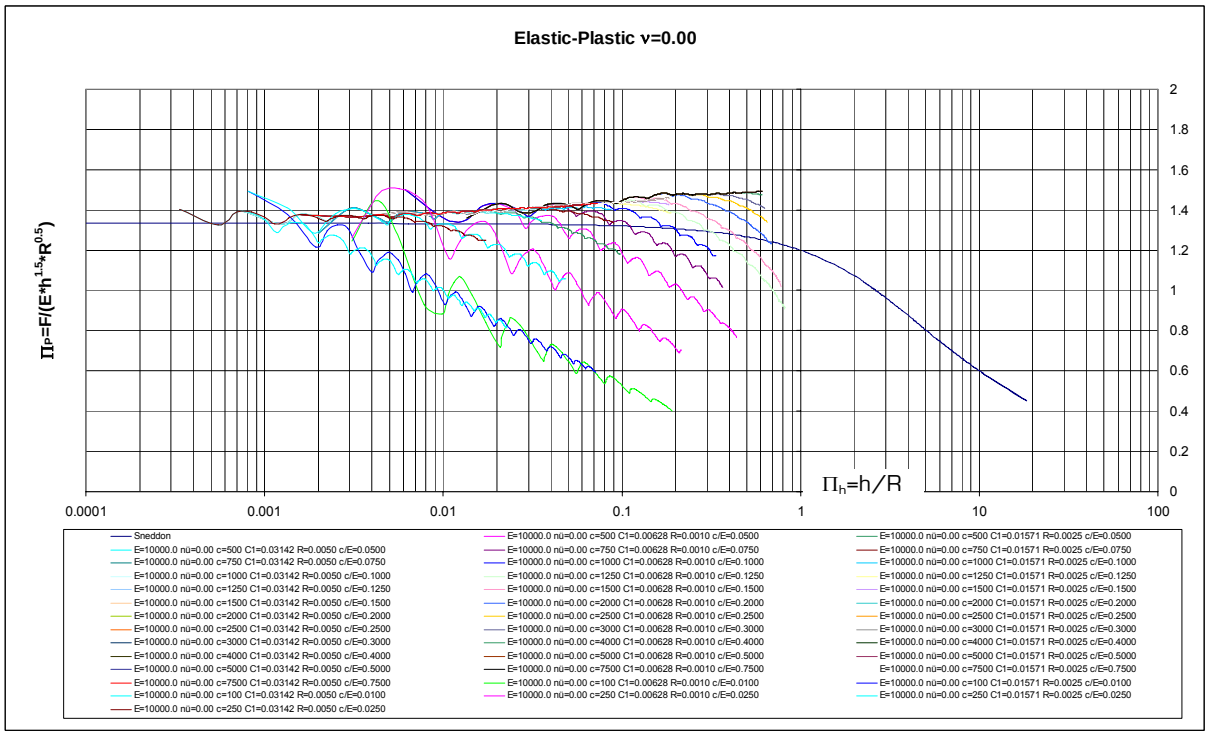

Figure 4-34 Dimensionless plot of numerical simulation results for elastic-plastic material for ν=0.0 and different c/E-ratios

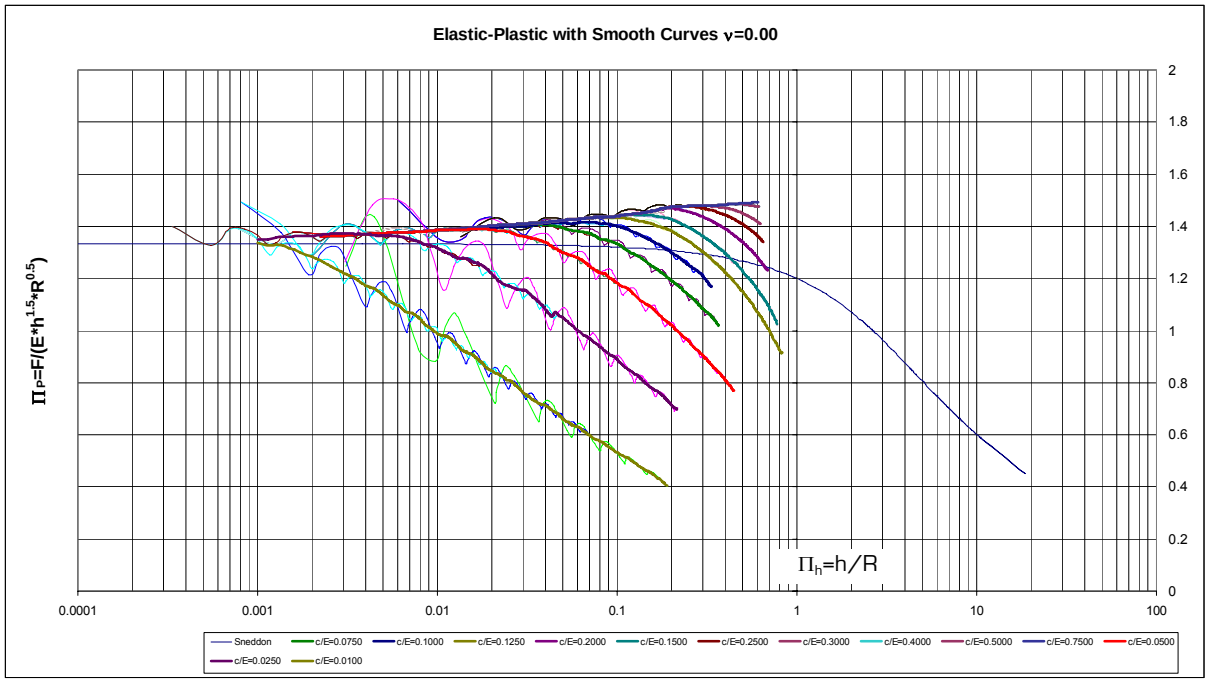

Figure 4-35 Dimensionless plot of smoothed and original numerical results for elastic-plastic material for ν=0.0 and different c/E-ratios

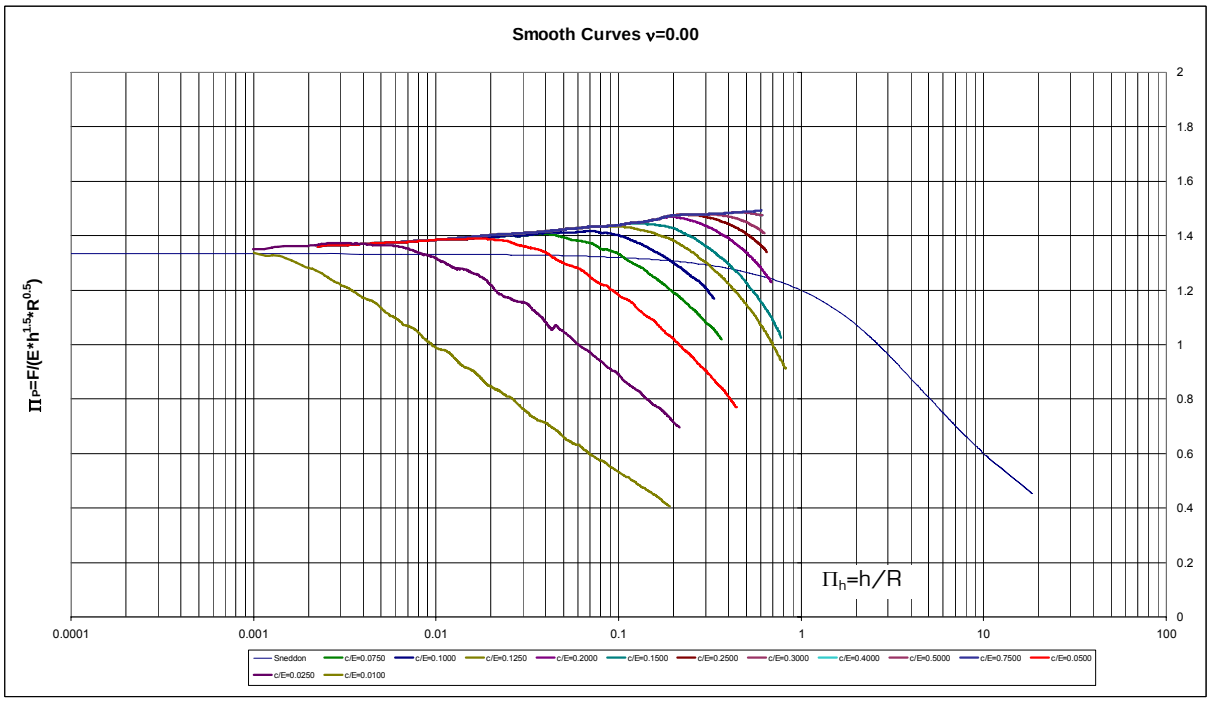

Figure 4-36 Dimensionless plot of smoothed numerical results for elastic-plastic material for ν=0.0 and different c/E-ratios

5 Discussion and concluding remarks

The identification of elastic material parameters from indentation tests of elasto-plastic materials is state of the art and commonly performed by using the so-called Oliver and Pharr Method [Oliver & Pharr 1992]. According to Oliver and Pharr 1992, Young's modulus of a material can be determined from the initial slope of the unloading curve of the load-penetration history. Herby, the exact shape of the indenter, obtained from a calibration procedure, and Poisson's ratio are required.

As regards identification of plastic material parameters, commonly the hardness of the material is employed for characterization of the inelastic behavior. The hardness is defined as the ratio of the maximum load and the contact area between tip and sample surface. Since the hardness depends on the tip shape, it is not a material parameter and cannot be used to describe the material behavior properly.

For identification of plastic material parameters (yield strength, etc.) from spherical indentation tests, the numerical results presented in this thesis can be used. With known tip shape (tip radius), Poisson's ratio, and Young's modulus, the yield strength of a material can be determined employing the following procedure:

1. Perform penetration test and record load and penetration continuously during loading and unloading;
2. Determine Young's modulus using the Oliver and Pharr method;
3. Compute Π_P and plot loading path of penetration test in dimensionless form as presented in Section 4;
4. Compare experimental result with results from numerical simulations presented in Section 4, giving access to the c/E-ratio of the considered material sample;
5. Compute deviatoric yield strength c using the c/E-ratio and the known Young's modulus.

The described procedure is illustrated for the identification of the yield strength of steel (St35). The results from spherical penetration tests on St35 were taken from [Kucharski and Mróz 2001]. Young's modulus of this material is 210000 N/mm² and Poisson's ratio is 0.3. According to [Kucharski and Mróz 2001] the tests are performed using a spherical indenter with a tip radius of 1.25 mm.

Figure 5-1 shows the dimensionless plot of the experimental results (red line) together with the results from numerical simulations for a Poisson's ratio of 0.3. The numerical results correspond to yield strength of 235, 355, 460 and 520 N/mm², giving c/E-ratios of 0.0011, 0.0017, 0.0022 and 0.0025, respectively.

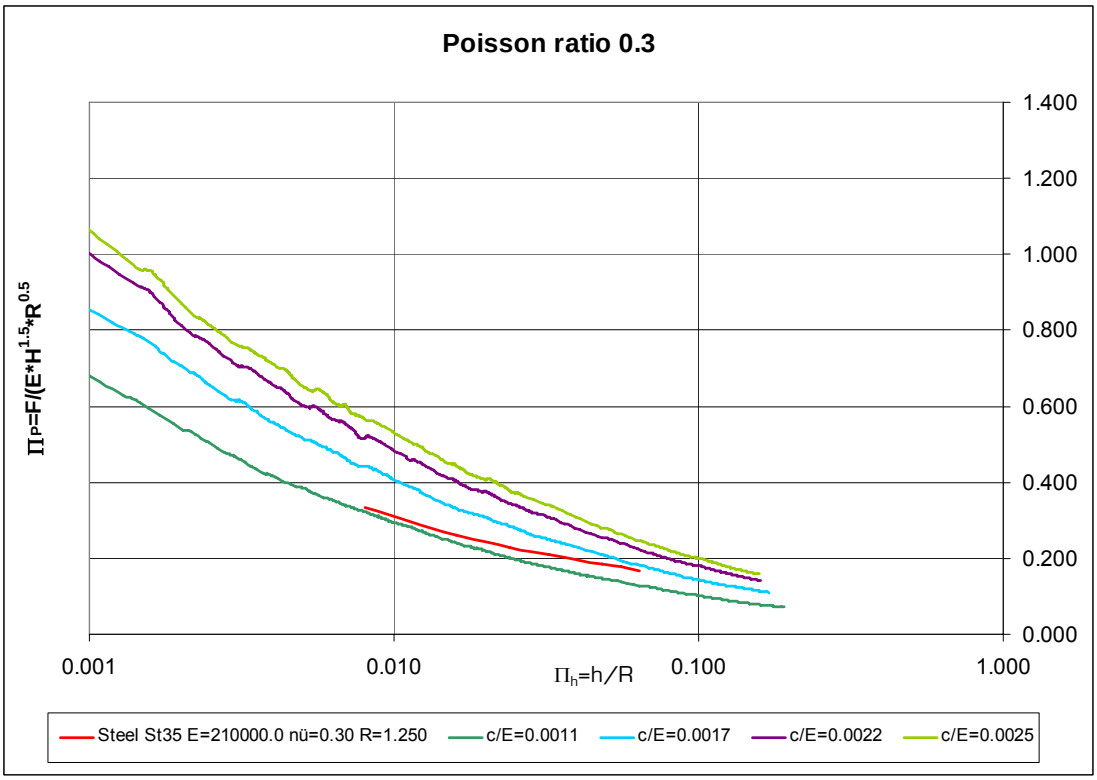

Figure 5-1 Comparison of numerical results (ν=0.3) and experimental results for St35

Comparing the numerical results with the experiment results indicates a c/E-ratio of the tested material between 0.0011 and 0.0017, giving a yield strength between 235 and 355 N/mm². This result is in good agreement with minimum yield strength of ST35, given by 235 N/mm². Since the exact yield

strength of the tested material is not known, the presented procedure seems to provide reasonable values for the yield strength of the tested steel.

At the beginning, spherical penetration is characterized by a pure elastic material response. However, after the onset of plastic deformation, elasto-plastic deformation occurs. The onset of plastic deformation depends on the tip radius as well as the material behavior in terms of Poisson's ratio, Young's modulus, and yield strength. The numerical results presented in Section 4, can be used to determine the onset of this plastic deformation, with materials exhibiting the same c/E-ratio and Poisson's ratio showing the same value of h/R indicating the first occurrence of plastic deformation. With this value of h/R at hand, the penetration depth corresponding to the onset of plastic deformation can be determined for a given tip radius (see Figures 5-2 to 5-6)

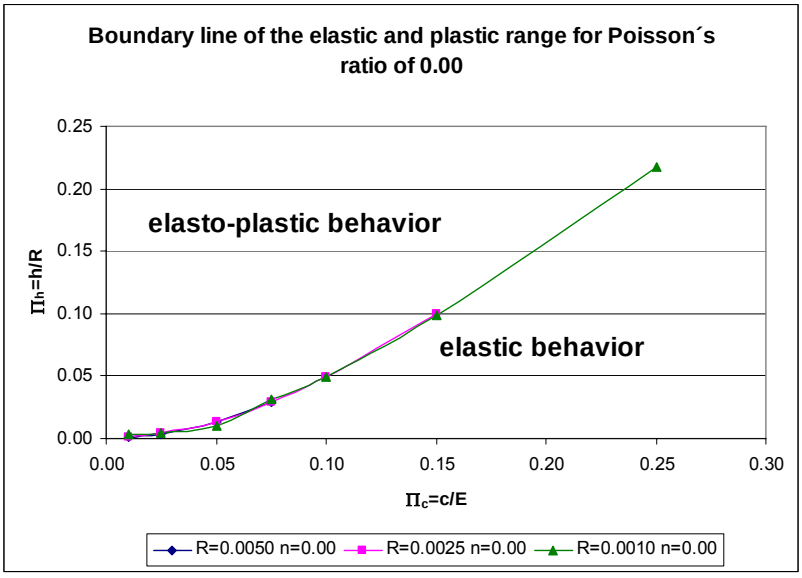

Figure 5-2 Elasto-plastic boundary line for ν=0.00

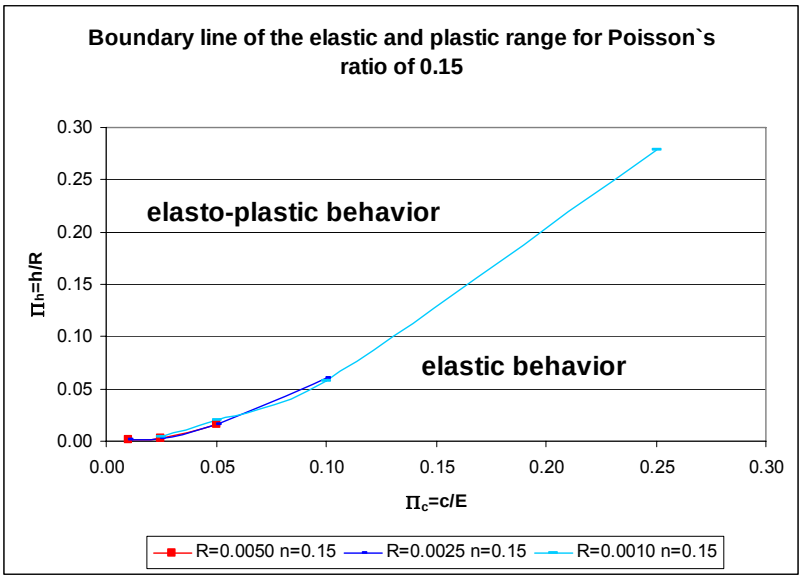

Figure 5-3 Elasto-plastic boundary line for ν=0.15

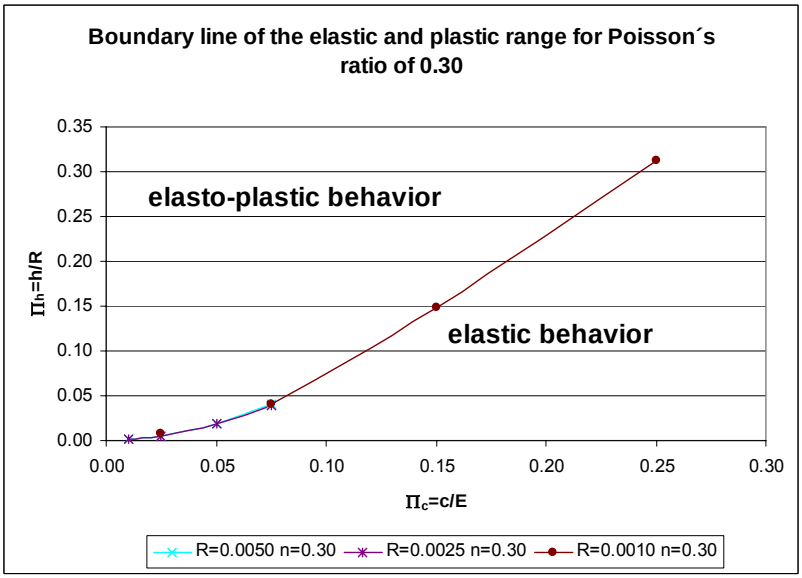

Figure 5-4 Elasto-plastic boundary line for ν=0.30

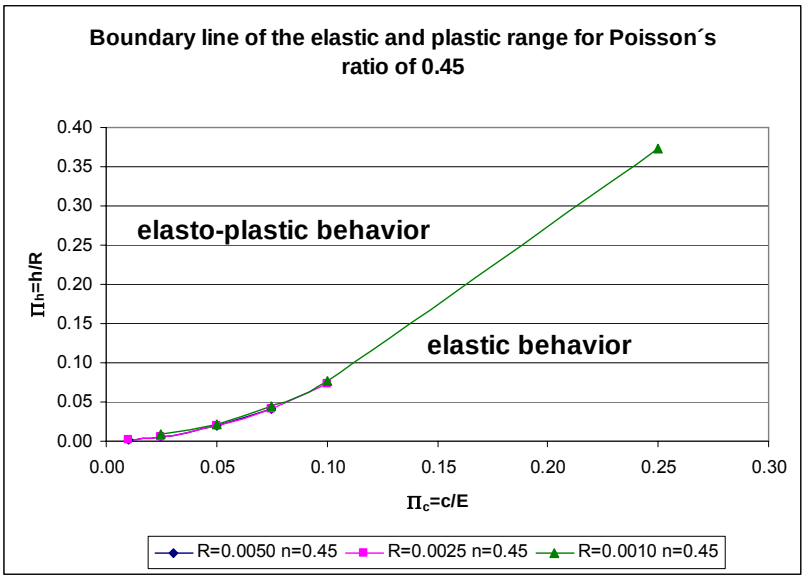

Figure 5-5 Elasto-plastic boundary line for ν=0.45

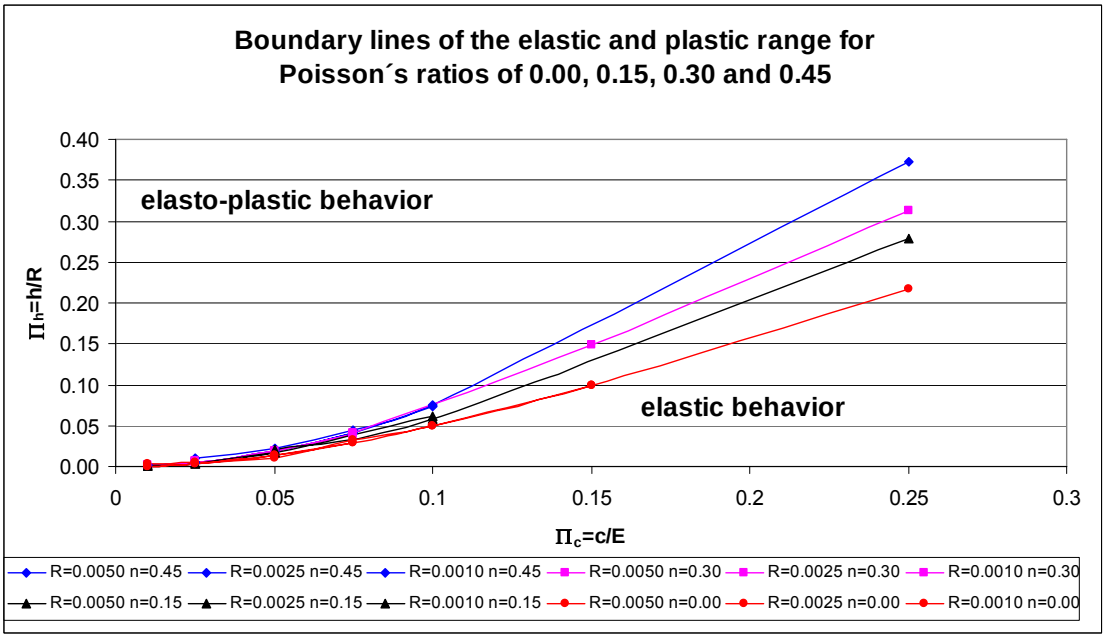

Figure 5-6 Comparison of the elasto-plastic boundary lines for ν=0.00, 0.15, 0.30, and 0.45

Based on the numerical results and the findings presented in this thesis, the following conclusions can be drawn:

1. Depending on tip shape, material properties, and maximum load, the spherical indentation process is characterized by either pure elastic or elasto-plastic material response. The onset of plastic deformation can be determined using the relation between the dimensionless parameters Π_h and Π_c defining the boundary line between elastic and elasto-plastic material response.
2. In case of penetration tests performed in the elastic regime, the presented modified Sneddon solution can be employed for identification of elastic material parameters. This modified analytical solution is based on the numerical simulations taking into account some effects neglected by the Sneddon solution, such as radial displacements of points at the contact surface.
3. If the elastic limit is exceeded, the indentation process is characterized by elasto-plastic material behavior. In this case, no analytical solutions, required for identification of plastic material properties, are available. However, plastic material parameters can be determined using the dimensionless representation of the numerical results presented in this thesis. This approach was illustrated for steel St35.

6 References

Cheng, L., Xia, X., Scriven, L., and Gerberich, W. (2005). Spherical-tip indentation of viscoelastic material. *Mechanics of Materials*, 37:213-226.

Graham, G. (1965). The contact 426 problem in the linear theory of viscoelasticity. *International Journal of Engineering Science*, 3(1):27-46.

Graham, G. (1967). Contact problem in linear theory of viscoelasticity when time dependent contact area has any number of maxima and minima. *International Journal of Engineering Science*, 5(6):495-514.

Hay, J.C., Bolshakov, A., and Pharr, G.M. (1999). A critical examination of the fundamental relations used in the analysis of nanoindentation data. *Journal of Material Research*, 14(6):2296-2305.

Hertz, H. (1882). Über die Berührung fester elastischer Körper. *Journal für die reine und angewandte Mathematik*, 92:156-171.

Hunter, S. (1960). The hertz problem for a rigid spherical indenter and a viscoelastic half-space. *Journal of the Mechanics and Physics of Solids*, 8(219-234).

Jäger, A., Lackner, R., and Eberhardsteiner, J. (2007). Identification of viscoelastic properties by means of nanoindentation taking the real tip geometry into account. *Meccanica*, 42:293-306.

Kucharski, S. and Mróz, Z. (2001). Identification of Hardening Parameters of Metals from Spherical Indentation Tests. *Journal of Engineering Materials and Technology*, Vol. 123:245-250.

Lee, E. (1955). Stress analysis in visco-elastic bodies. *Quarterly of Applied Mathematics*, 13:183-190.

Lee, E. and Radok, J. (1960). The contact problem for viscoelastic bodies. *Journal of Applied Mechanics*, 27:438-444.

Oliver, W. and Pharr, G. (1992). An improved technique for determining hardness and elastic modulus using load and displacement sensing indentation experiments. *Journal of Materials Research*, 7(6):1564-1583.

Pichler Ch. (2007). Multiscale characterization and modeling of creep and autogeneous shrinkage of early-age cement-based materials. PhD thesis, Vienna University of Technology, Vienna.

Radok, J. (1957). Visco-elastic stress analysis. *Quarterly of Applied Mathematics*, 15:189-202.

Sneddon, I. (1965). The relation between load and penetration in the axisymmetric Boussinesq problem for a punch of arbitrary profile. *International Journal of Engineering Science*, 3:47-57.

Ting, T. (1966). The contact stress between a rigid indenter and a viscoelastic half-pace. *Journal of Applied Mechanics*, 33:845-854.

Ting, T. (1968). Contact problems in linear theory of viscoelasticity. *Journal of Applied Mechanics*, 35:248-254.

Vandamme, M. and Ulm, F.-J. (2006). Viscoelastic solutions for conical indentation. *International Journal of Solids and Structures*, 43(10):3142-3165.